ANNUAL REVIEWS

Annual Review of Earth and Planetary Sciences

Forming Planets via Pebble Accretion

Anders Johansen[1] and Michiel Lambrechts[2]

[1]Lund Observatory, Lund University, 221 00 Lund, Sweden; email: anders@astro.lu.se

[2]Laboratoire Lagrange, Observatoire de la Côte d'Azur, Université Côte d'Azur, 06304 Nice Cedex 4, France; email: michiel.lambrechts@oca.eu

Annu. Rev. Earth Planet. Sci. 2017. 45:359–87

The *Annual Review of Earth and Planetary Sciences* is online at earth.annualreviews.org

https://doi.org/10.1146/annurev-earth-063016-020226

Keywords

planetary systems, formation of planets and satellites, gaseous planets, planet-disk interactions, protoplanetary disks

Abstract

The detection and characterization of large populations of pebbles in protoplanetary disks have motivated the study of pebble accretion as a driver of planetary growth. This review covers all aspects of planet formation by pebble accretion, from dust growth over planetesimal formation to the accretion of protoplanets and fully grown planets with gaseous envelopes. Pebbles are accreted at a very high rate—orders of magnitude higher than planetesimal accretion—and the rate decreases only slowly with distance from the central star. This allows planetary cores to start their growth in much more distant positions than their final orbits. The giant planets orbiting our Sun and other stars, including systems of wide-orbit exoplanets, can therefore be formed in complete consistency with planetary migration. We demonstrate how growth tracks of planetary mass versus semimajor axis can be obtained for all the major classes of planets by integrating a relatively simple set of governing equations.

1. INTRODUCTION

Better a diamond with a flaw than a pebble without.
—Chinese proverb, traditionally attributed to Confucius (551–479 BC)

The role of solid particles in planet formation has been recognized at least back to the original formulation of the planetesimal hypothesis (Chamberlin 1916), which states that the planets formed from collisions between smaller planetesimals akin to the asteroids in the asteroid belt. A mathematically and physically strict version of the planetesimal hypothesis was developed by Viktor Safronov during the 1950s and 1960s and was summarized in his book *Evoliutsiia Doplanetnogo Oblaka* (*The Evolution of the Protoplanetary Cloud*) (Safronov 1969). In this monumental work, all the stages of planet formation were laid out and explored—the formation of the protoplanetary disk, the coagulation and sedimentation of dust particles to form pebbles, the formation of planetesimals by gravitational instability in the dust layer, and the growth of planetary objects by planetesimal accretion. There is now, almost five decades after Safronov's book, overwhelming confirmation that accumulation of solids plays the dominant role in planet formation. Observations of protoplanetary disks in millimeter and centimeter wavelengths show that micrometer-sized dust grains grow to pebble sizes around virtually all young stars (Testi et al. 2003, Wilner et al. 2005). The asteroids and Kuiper belt objects, and their debris disk counterparts around other stars (Wyatt 2008), are all remnants of the planetesimals that are the starting seeds of planetary bodies (Johansen et al. 2014). The correlation between stellar metallicity and the occurrence rate of close-in giant planets provides cornerstone evidence that accumulation of solids is crucial even for the formation of giant planets whose masses are dominated by hydrogen and helium gas (Santos et al. 2004, Fischer & Valenti 2005, Buchhave et al. 2012).

The core accretion scenario was developed to explain the formation of giant planets within the planetesimal hypothesis (Mizuno 1980, Stevenson 1982, Lissauer 1987, Pollack et al. 1996). The core forms by accretion of planetesimals, which must be provided dynamically cold in order to obtain the highest growth rate. The gaseous envelope contracts after the core reaches its isolation mass with respect to planetesimals and the accretion luminosity of the core is reduced; the core finally undergoes runaway gas accretion after the envelope has grown to be more massive than the core. The core accretion scenario has been very successful in explaining the inferred core masses of the giant planets in the Solar System (Mizuno 1980, Stevenson 1982). Core accretion nevertheless faces two major obstacles. First, very high column densities of planetesimals are required to build the observed core masses of Jupiter and Saturn within their planetesimal feeding zones (Pollack et al. 1996). This raises concerns about the formation and fate of the 80–90% of the planetesimals that are not used to build these cores. Planetesimal accretion rates drop sharply with distance from the Sun, so the cores of Uranus and Neptune are very challenging to form within the lifetime of the protoplanetary disk (as was pointed out by Safronov 1969). Second, the assumption that cores grow in isolation from other cores and can accrete planetesimals of negligible velocity dispersion has been shown in dynamical simulations of the formation of multiple cores to not be justifiable (Levison et al. 2010). Scattering in encounters between planetesimals and cores leads to excitation of planetesimal orbits and core growth rates that are much too low to reach substantial masses while there is still gas left in the protoplanetary disk. These issues have spawned interest in the alternative view that planets form by gravitational instability in the gas (Cameron 1978, Boss 2001, Mayer et al. 2002, Nayakshin 2010).

This review focuses on a relatively newly discovered mechanism for boosting the accretion rate of solids in the core accretion scenario, namely pebble accretion. Pebble accretion revolves around millimeter-to-centimeter-sized pebbles as the fundamental drivers of planetary growth.

Pebbles are accreted by a growing protoplanet much more readily than planetesimals, owing to energy dissipation by gas drag as the pebble passes the protoplanet (Johansen & Lacerda 2010, Ormel & Klahr 2010). Pebbles that couple frictionally to the gas on a timescale similar to the characteristic time to pass the region of gravitational influence of the protoplanet—the Bondi radius of the sub-Keplerian gas flow for planetesimals and the Hill radius for protoplanets—are accreted from the entire gravitational reach of the planet. This results in planetary growth rates that are several orders of magnitude higher than even the most optimistic planetesimal accretion rates (Lambrechts & Johansen 2012).

Disk aspect ratio: the gas scale-height H divided by the semimajor axis r

The timing of the development of the pebble accretion mechanism was linked to the observational detection of large amounts of pebbles in protoplanetary disks (Testi et al. 2003, Wilner et al. 2005). These observations were in turn aligned with the growing realization that several barriers hamper dust coagulation in protoplanetary disks—particularly the bouncing, fragmentation, and drift barriers (Brauer et al. 2007, Blum & Wurm 2008, Brauer et al. 2008, Zsom et al. 2010). These barriers make protoplanetary disks very efficient factories for producing pebbles of millimeter to centimeter sizes. The presence of pebbles in protoplanetary disks can also explain how planetesimals form, as many mechanisms have been identified to concentrate such particles in the turbulent gas, including the streaming instability (see reviews by Chiang & Youdin 2010, Johansen et al. 2014). The gravitational collapse of these overdense pebble filaments typically leads to the formation of large planetesimals (Johansen et al. 2007, 2015; Simon et al. 2016), matching qualitatively the 100-km-scale birth sizes of asteroids inferred by Bottke et al. (2005) and Morbidelli et al. (2009) as necessary to match the current observed size distribution of asteroids. The largest planetesimals can then continue to grow by accreting other planetesimals as well as pebbles left over from planetesimal formation.

Pebble accretion rates are determined by the dominant size of pebbles in protoplanetary disks. The contribution of planetesimal accretion is important as well, particularly to drive the growth from planetesimals to protoplanets. Therefore this review focuses on all stages of planet formation: the growth of pebbles and the formation of planetesimals (Section 2), planetesimal accretion rates (Section 3), and pebble accretion rates (Section 4). In Section 5 we connect all these physical aspects of planetary growth to produce growth tracks for the major classes of planets: gas giants, ice giants, wide-orbit exoplanets, and super-Earths, as well as the protoplanets that feed terrestrial planet formation. We outline important priorities for future research on planet formation in Section 6.

1.1. A Note on Protoplanetary Disk Parameters

The governing equations of planet formation by pebble accretion depend strongly on the physical state of the protoplanetary disk, such as its gas column density and temperature. Many of these parameters vary considerably with both distance from the central star and time. In this review we choose to scale the presented equations in terms of parameters that have only little variation with semimajor axis. These parameters are as follows.

1.1.1. The disk aspect ratio H/r. The disk aspect ratio determines the temperature T through the relation

$$\frac{H}{r} = \frac{c_s}{v_K} \propto T^{1/2}. \quad (1)$$

Here c_s is the gas sound speed and v_K is the Keplerian speed. The aspect ratio flares slightly, with $H/r = 0.033\,(r/\mathrm{AU})^{1/4}$, in the optically thin model of Hayashi (1981), whereas full radiative transfer models presented by Bitsch et al. (2015a) yield an aspect ratio that is flat out to 5–10 AU and then increases approximately as $r^{2/7}$ further out where stellar irradiation dominates the

heating (Chiang & Youdin 2010). The aspect ratio in the inner disk is approximately 0.05 during the first million years of disk evolution, when viscous heating is significant, but then drops to approximately 0.02–0.03 in the later disk stages (Bitsch et al. 2015a). This drop has important consequences for the formation of super-Earths with low-mass gaseous envelopes (Section 5.6).

Sub-Keplerian speed (Δv): defined as (minus) the difference between the gas orbital speed v_g and the Keplerian speed v_K

1.1.2. The sub-Keplerian speed Δv. Radial pressure support causes the gas to orbit at a sub-Keplerian speed $v_g = v_K - \eta v_K = v_K - \Delta v$. The radial pressure parameter η is given in terms of the radial pressure gradient through $\eta \equiv -(1/2)(H/r)^2(\partial \ln P/\partial \ln r)$. That definition in turn gives

$$\Delta v = -\frac{1}{2}\frac{H}{r}\frac{\partial \ln P}{\partial \ln r} c_s. \tag{2}$$

In the optically thin approach of Hayashi (1981) the sub-Keplerian speed lies at a constant value of $\Delta v \approx 50$ m s^{-1} through the protoplanetary disk. Radiative transfer models of protoplanetary disks are much colder than the optically thin model, and this results in lower values of Δv. The simulations of Bitsch et al. (2015a) display $\Delta v \approx 30$ m s^{-1} in large regions of the protoplanetary disk.

1.1.3. Column density fractions of gas f_g, pebbles f_p, and planetesimals f_{pla}. We use generic profiles for the column densities of gas Σ_g, pebbles Σ_p, and planetesimals Σ_{pla},

$$\Sigma_g = 10^4 \,\mathrm{kg\,m^{-2}}\, f_g \left(\frac{r}{\mathrm{AU}}\right)^{-1}, \tag{3}$$

$$\Sigma_p = 0.01\, f_p \Sigma_g, \tag{4}$$

$$\Sigma_{pla} = 0.01\, f_{pla} \Sigma_g. \tag{5}$$

Here, f_g, f_p and f_{pla} are parameterizations of the column density of the protoplanetary disk relative to the standard profile. We choose nominal values of the disk parameters f_g, f_p and f_{pla} from the simulations of Bitsch et al. (2015a). Here, $f_g = 1$ represents a young protoplanetary disk of accretion rate $\dot{M} \sim 10^{-7} M_\odot\,\mathrm{yr}^{-1}$, and $f_g = 0.1$ is representative of an evolved protoplanetary disk of age one to several million years. Actual fits to the disk profiles that result from radiative transfer simulations can be found in the appendix of Bitsch et al. (2015a). Note that we use either natural units or SI units in this review.

1.1.4. Particle midplane layer thickness ratio H_p/H. The scale-height of the particle midplane layer H_p determines the midplane particle density through $\rho_p = \Sigma_p/(\sqrt{2\pi} H_p)$. The thickness is set as a balance between sedimentation and turbulent diffusion (for details, see the review by Johansen et al. 2014). The ratio relative to the gas scale-height can acquire values between 1 (unsedimented) and 0.01 (when stirred by midplane turbulence alone). We use a generic value of $H_p/H = 0.1$ in this review.

2. PEBBLE GROWTH AND PLANETESIMAL FORMATION

In this section we briefly review dust coagulation and planetesimal formation. We focus on describing practical recipes that can be used to calculate the pebble sizes needed for pebble accretion simulations. We refer the reader to many recent review articles on dust growth and planetesimal formation for details (Blum & Wurm 2008, Chiang & Youdin 2010, Testi et al. 2014, Johansen et al. 2014, Birnstiel et al. 2016).

2.1. Coagulation

The main stage of particle coagulation occurs in the dense and relatively long-lived protoplanetary disk. These protoplanetary disks have typical sizes between 100 and 1,000 AU (Andrews et al. 2009) and accrete mass onto their central star at a rate that declines from approximately $10^{-7} M_\odot\,\mathrm{yr}^{-1}$ to $10^{-9}\ M_\odot\,\mathrm{yr}^{-1}$ over the few-million-year lifetime of the protoplanetary disk (Hartmann et al. 1998).

Coagulation: the growth of pebbles by mutual sticking

Stokes number: the particle friction time multiplied by the orbital frequency Ω

Epstein regime: aerodynamical friction regime where gas molecules recoiling from a collision with a dust grain move much further than the grain size before colliding with another gas molecule

2.2. Pebble Sizes

The efficiency of pebble accretion depends on the aerodynamical friction time τ_f of the pebbles. The Stokes number of a particle of radius R and internal density $\rho_\bullet$ moving in a gas of column density Σ_g is defined as

$$\mathrm{St} = \Omega\tau_\mathrm{f} = \frac{\sqrt{2\pi}\,R\rho_\bullet}{\Sigma_\mathrm{g}} = 2.5\times10^{-4}\,f_\mathrm{g}^{-1}\left(\frac{R}{10^{-3}\,\mathrm{m}}\right)\left(\frac{\rho_\bullet}{10^{3}\,\mathrm{kg\,m^{-3}}}\right)\left(\frac{r}{\mathrm{AU}}\right). \quad (6)$$

We assumed here that the particle is in the midplane of the protoplanetary disk and that the friction is in the Epstein regime (see Johansen et al. 2014 for a discussion of friction regimes). The Stokes number also determines the turbulent collision speed v_c of particles with $\mathrm{St} < 1$ (Ormel & Cuzzi 2007) through the expression

$$v_\mathrm{c} = \sqrt{3}\sqrt{\alpha}\sqrt{\mathrm{St}}c_\mathrm{s}. \quad (7)$$

Here, α is a nondimensional measure of the turbulent viscosity and c_s is the sound speed of the gas.

The temporal evolution of the particle size distribution can be modeled by solving the coagulation equation in discrete particle bins or by using statistical particle methods (Brauer et al. 2007, Ormel et al. 2007, Zsom & Dullemond 2008). The results of such simulations can typically be understood in terms of growth to one of the three coagulation barriers: (*a*) fragmentation barrier, (*b*) bouncing barrier, and (*c*) radial drift barrier.

2.2.1. Fragmentation barrier. The Stokes number of the fragmentation barrier is obtained by setting the collision speed v_c equal to a critical fragmentation speed u_f (Birnstiel et al. 2011). This yields the expression

$$\mathrm{St} = \frac{u_\mathrm{f}^2}{3\alpha c_\mathrm{s}^2} = 0.015\left(\frac{\alpha}{10^{-3}}\right)^{-1}\left(\frac{u_\mathrm{f}}{10\,\mathrm{m\,s^{-1}}}\right)^{2}\left(\frac{H/r}{0.05}\right)^{-2}\left(\frac{r}{\mathrm{AU}}\right)^{2}. \quad (8)$$

The fragmentation threshold is, in reality, a complicated function of the porosity and relative size of impactor and target (Wurm et al. 2005, Güttler et al. 2010). But, for simplicity, one can set u_f to be a constant to obtain an approximate expression for the fragmentation barrier.

2.2.2. Bouncing barrier. Compact particles will only stick below a threshold speed that decreases with the mass of the particles. This leads to a bouncing barrier at smaller particle sizes than the fragmentation barrier. Zsom et al. (2010) demonstrated that the bouncing barrier in massive protoplanetary disks (similar to or more massive than the minimum mass solar nebula model of Hayashi 1981) arises at particle masses of approximately 10^{-3} kg, as particles that grew first as fluffy aggregates become compactified in collisions. Compact particles are in turn more prone to bouncing than sticking. However, the more relevant case of protoplanetary disks with column densities below the minimum mass solar nebula yields a bouncing barrier when the turbulent

collision speed is equal to the sticking speed

$$v_s = \sqrt{\frac{5\pi a_0 F_{\rm roll}}{m}}. \quad (9)$$

Monomer: basic building block of dust aggregates, typically assumed μm in size

Here, a_0 is the monomer size, $F_{\rm roll}$ is the force needed to roll a monomer over the surface of another monomer, and m is the reduced mass of the colliding dust aggregates (Güttler et al. 2010). This gives the Stokes number expression

$$\begin{aligned}{\rm St} &= \left[\frac{15(2\pi)^{3/2} a_0 F_{\rm roll}\rho_\bullet^2}{6\alpha c_s^2 \Sigma_g^3}\right]^{1/4} = 3.7\times10^{-6} f_g^{-3/4}\left(\frac{a_0}{\mu{\rm m}}\right)^{1/4}\left(\frac{F_{\rm roll}}{8.5\times10^{-10}\,{\rm N}}\right)^{1/4} \\ &\times\left(\frac{\rho_\bullet}{3500\,{\rm kg\,m^{-3}}}\right)^{1/2}\left(\frac{\alpha}{10^{-3}}\right)^{-1/4}\left(\frac{H/r}{0.05}\right)^{-1/2}\left(\frac{r}{\rm AU}\right). \quad (10)\end{aligned}$$

The bouncing barrier is clearly very severe for compact silicate particles (for which we scaled the rolling force). Water ice has much higher surface energy than silicates and hence ice aggregates resist compactification in collisions (Wada et al. 2009). The high sticking efficiency of porous particles can lead to the formation of very large aggregates, limited in growth only by their radial drift (discussed in the following section), outside of the water ice line (which is situated at disk temperatures of approximately 180 K, typically 1–3 AU from the star; see discussion in Martin & Livio 2012, Morbidelli et al. 2016).

2.2.3. Radial drift barrier. Particles with properties that avoid the bouncing and fragmentation barriers, for example very fluffy ice particles (Wada et al. 2009), still face the formidable radial drift barrier. The radial drift barrier is encountered when the growth timescale $\mathrm{St}/\dot{\mathrm{St}}$ equals the radial drift timescale $r/\dot{r}$. That gives a Stokes number of

$${\rm St} = \frac{\sqrt{3}}{8}\frac{v_K}{\Delta v}\frac{\Sigma_p}{\Sigma_g} = 0.53\left(\frac{\Delta v}{50\,{\rm m\,s^{-1}}}\right)^{-1}\frac{\Sigma_p/\Sigma_g}{0.01}\left(\frac{r}{\rm AU}\right)^{-1/2}. \quad (11)$$

This expression for the Stokes number at the drift barrier was derived analytically by Birnstiel et al. (2012) and Lambrechts & Johansen (2014). Lambrechts & Johansen (2014) calculated the column density of the drifting pebbles, based on the concept of an outward-moving pebble formation front. The column density of drifting pebbles turns out to be significantly lower than the canonical 1% of the gas column density, a consequence of the high radial drift speed of the pebbles. This also lowers the Stokes number of the drifting pebbles through the column-density dependence in Equation 11.

2.3. Planetesimal Formation

Radial drift sets a natural limit to the maximum particle sizes that can be obtained by coagulation, even if particles would stick perfectly in collisions. Particles can, in principle, break through the radial drift barrier inside a pressure bump where the radial drift vanishes (Drążkowska et al. 2013), or they can break through owing to the very efficient sticking of extremely fluffy ice particles with internal density of down to 10^{-5} times the material density (Okuzumi et al. 2012). However, the prevalence of pressure bumps and the formation of extremely fluffy ice particles are still under exploration (see, e.g., Krijt et al. 2015, who found that fluffy ice particles are eroded by collisions with single monomers).

The self-gravity of the pebble component can help in the formation of planetesimals by gravitational instability, but particle densities in excess of 100 times the gas density are needed to initiate a gravitational collapse. The streaming instability provides a pathway to planetesimal formation

by concentrating the pebbles in the protoplanetary gas disk into dense filaments that collapse under self-gravity (Youdin & Goodman 2005, Johansen & Youdin 2007, Youdin & Johansen 2007). The emergence of dense pebble filaments happens above a threshold metallicity (defined as the pebble column density relative to the gas) of approximately 1.5% at St $\sim$ 0.1 (Johansen et al. 2009, Bai & Stone 2010), increasing toward both smaller and larger particles (Carrera et al. 2015). Drążkowska & Dullemond (2014) demonstrated that coagulation can produce pebble sizes that trigger the streaming instability outside of the water ice line, while the bouncing barrier for silicates interior of the water ice line stalls particle growth below sizes where the streaming instability does not operate under nominal metallicities.

Including particle self-gravity in streaming instability simulations leads to the formation of planetesimals of a wide range of sizes, following the approximate differential mass distribution

$$\frac{\mathrm{d}N}{\mathrm{d}M} \propto M^{-1.6} \exp[-(M/M_{\mathrm{exp}})^{\beta}]. \quad (12)$$

The power law exponent of -1.6 was found in independent simulations by Johansen et al. (2015) and Simon et al. (2016). Schäfer et al. (2017) used large-box simulations to infer a steepness parameter β for the exponential cutoff in the range $\beta \approx 0.3 \ldots 0.4$. The exponential cutoff mass M_{exp} corresponds to a typical planetesimal size of approximately 100 km in radius for nominal particle column densities. This characteristic planetesimal birth size is in good agreement with the observed bumps at 100 km in diameter in the size distribution of asteroids and Kuiper belt objects (Bottke et al. 2005, Morbidelli et al. 2009, Sheppard & Trujillo 2010). Simulations used to measure the initial mass function of planetesimals nevertheless considered the streaming instability to operate in isolation. The relative roles of the streaming instability and other instabilities that are active in the planet-forming regions of the protoplanetary disk, such as the vertical shear instability (Nelson et al. 2013, Lin & Youdin 2015) and baroclinic instabilities (Raettig et al. 2013), are still poorly understood and should be an important priority for future research.

3. PLANETESIMAL ACCRETION

The classical core accretion scenario for the formation of giant planets considers planetesimals as the only contributors to the core mass. Pollack et al. (1996) divided the formation of a giant planet into three phases. Phase I is the growth of the core to its isolation mass. This phase takes just 1 Myr at 5 AU in a protoplanetary disk whose column density of planetesimals is enhanced by a factor of six over the value in the minimum mass solar nebula. The enhancement is needed to increase the isolation mass to approximately 10 $M_{\oplus}$, similar to the inferred core masses for the giant planets in the Solar System (Guillot 2005), and to achieve an accretion timescale in accordance with the lifetime of the protoplanetary disk. The core begins to attract a gaseous envelope whose mass increases nonlinearly with the core mass at this stage (Mizuno 1980, Stevenson 1982, Ikoma et al. 2000, Piso & Youdin 2014). The cross section for planetesimal accretion is increased slightly by ablation of planetesimals in the growing envelope (Hayashi et al. 1985, D'Angelo et al. 2014). Phase II is entered when the isolation mass is reached. The atmosphere can now contract faster, owing to the reduced heating by infalling planetesimals. This phase can take up to 10 Myr unless planetesimal accretion is reduced or stopped artificially. Phase III is reached when the core mass and envelope mass are comparable (the crossover mass); this triggers runaway accretion of gas from the protoplanetary disk.

3.1. Core Accretion Rate

We are mainly concerned here with the accretion timescale of the core, as a comparison to the accretion rate that can be obtained with pebble accretion (discussed in Section 4). Excellent reviews

with details on planetesimal accretion can be found in Benz et al. (2014) and Helled et al. (2014). The accretion rate of planetesimals is given in its most general form by

$$\frac{\mathrm{d}M}{\mathrm{d}t} = \pi R^2 \rho_{\mathrm{pla}} v_{\mathrm{pla}} \left[1 + \left(\frac{v_{\mathrm{e}}}{v_{\mathrm{pla}}}\right)^2\right]. \quad (13)$$

Gravitational focusing: increase in accretion cross section due to the bending of planetesimal trajectories by the gravity of the core

Hill speed: the speed of the Keplerian shear at the edge of the Hill radius; a 1-$M_\oplus$ protoplanet at 5 AU has a Hill speed of approximately 130 m s^{-1}

Here M and R are the mass and the radius of the core, ρ_{pla} is the local planetesimal swarm density, v_{pla} is the approach speed of the planetesimals, and v_{e} is the escape speed from the surface of the core, giving rise to gravitational focusing.

3.2. Planetesimal Dynamics

The dynamical state of the planetesimal component determines both the scale-height of the planetesimals and their approach speed to the core. There are two fundamental regimes of planetesimal dynamics and core growth—dispersion-dominated growth (Safronov 1969) and shear-dominated growth (Greenberg et al. 1991). The dispersion-dominated regime is most easily treated, as planetesimals have random velocities v_{ran} that are much larger than the Hill speed $v_{\mathrm{H}} = \Omega R_{\mathrm{H}}$, with R_{H} denoting the Hill radius. In this case, the random speed determines both the scale-height of the planetesimals and the approach speed to the core. In the shear-dominated case, the approach speed is set by the Hill speed. We put the two regimes here into a general equation,

$$\frac{\mathrm{d}M}{\mathrm{d}t} = \pi R^2 \Sigma_{\mathrm{pla}} \Omega \frac{v_{\mathrm{pla}}}{v_{\mathrm{ran}}} \left[1 + \left(\frac{v_{\mathrm{e}}}{v_{\mathrm{pla}}}\right)^2\right], \quad (14)$$

with $v_{\mathrm{pla}} = \max(v_{\mathrm{ran}}, v_{\mathrm{H}})$. That gives the two limits

$$\frac{\mathrm{d}M}{\mathrm{d}t} = \pi R^2 \Sigma_{\mathrm{pla}} \Omega \left[1 + \left(\frac{v_{\mathrm{e}}}{v_{\mathrm{ran}}}\right)^2\right] \quad \text{for} \quad v_{\mathrm{ran}} \gg v_{\mathrm{H}} \quad \text{(dispersion) and} \quad (15)$$

$$\frac{\mathrm{d}M}{\mathrm{d}t} = \pi R^2 \Sigma_{\mathrm{pla}} \frac{v_{\mathrm{H}}}{v_{\mathrm{ran}}} \Omega \left[1 + \left(\frac{v_{\mathrm{e}}}{v_{\mathrm{H}}}\right)^2\right] \quad \text{for} \quad v_{\mathrm{ran}} \ll v_{\mathrm{H}} \quad \text{(shear)}. \quad (16)$$

The shear-dominated case is complicated by the fact that planetesimals arriving with similar semimajor axes as the core go on horseshoe orbits that do not enter the Hill sphere. However, Greenberg et al. (1991) demonstrated that the trajectories of planetesimals on orbits near the edge of the Hill sphere are bent by a combination of the gravity of the core and the Coriolis force, so the approach speed past the core can be taken to be approximately equal to the Hill speed.

In the limit of strong gravitational focusing, $v_{\mathrm{e}} \gg v_{\mathrm{pla}}$, we get the combined expression

$$\frac{\mathrm{d}M}{\mathrm{d}t} = \pi R^2 \Sigma_{\mathrm{pla}} \Omega \frac{6p^{-1}}{\max(\zeta, 1)\zeta}. \quad (17)$$

Here, $\zeta \equiv v_{\mathrm{ran}}/v_{\mathrm{H}}$ determines the accretion regime and $p \equiv R/R_{\mathrm{H}}$ is the size of the core relative to its Hill radius. The latter can be written as

$$p = \frac{R}{R_{\mathrm{H}}} = \left(\frac{4\pi G \rho_\bullet}{9\Omega^2}\right)^{-1/3} \approx 0.001 \left(\frac{r}{5\,\mathrm{AU}}\right)^{-1} \left(\frac{\rho_\bullet}{2 \times 10^3\,\mathrm{kg\,m^{-3}}}\right)^{-1/3}. \quad (18)$$

That gives the growth rate

$$\frac{\mathrm{d}M}{\mathrm{d}t} \approx 3.8\,\mathrm{M_\oplus\,Myr^{-1}}\, f_{\mathrm{pla}} \left(\frac{M}{\mathrm{M_\oplus}}\right)^{2/3} \left(\frac{r}{5\,\mathrm{AU}}\right)^{-1.5} [\max(\zeta, 1)\zeta]^{-1}. \quad (19)$$

The timescale to build up a core of mass M (which must reach $10\,M_\oplus$ to agree with the inferred core masses of gas giants and ice giants) is then

$$t_{\rm pla} = 1.7\,{\rm Myr}\, f_{\rm pla}^{-1} \left(\frac{M}{10\,M_\oplus}\right)^{1/3} \left(\frac{r}{5\,{\rm AU}}\right)^{1.5} [\max(\zeta, 1)\zeta]. \quad (20)$$

For planetesimals that are not affected by gas drag, typically those with $R_{\rm pla} \gg 1$ km, ζ will not be less than unity. This constraint arises because a single strong scattering of a planetesimal on a circular orbit already induces $\zeta \approx 1$ (Rafikov 2004) and ζ subsequently rises slowly. Greenzweig & Lissauer (1990) found planetesimal eccentricities generally between two and six times the Hill eccentricity $e_{\rm H} = v_{\rm H}/v_{\rm K}$ after a scattering event ($e/e_{\rm H} = v_{\rm ran}/v_{\rm H} = \zeta$). Pollack et al. (1996) assumed, on the contrary, that the velocity dispersion of the planetesimals is set mainly by internal scattering within the planetesimal swarm, motivating them to consider a velocity dispersion equal to the escape speed of the largest planetesimals. The actual value of ζ as a function of time must be followed in a computer simulation that evolves the orbital elements of the planetesimal swarm as a result of interactions with both planetesimals and the growing core. D'Angelo et al. (2014) used stirring formulae calibrated with N-body simulations and found planetesimal eccentricities up to 0.03 near the core, which decreased toward the edge of the feeding zone. This translated in turn to random speeds on the order of 100 m s^{-1} or ζ of approximately unity or higher. However, these simulations considered the formation of a single giant planet and hence did not take into account the possibility that the planetesimals can get their orbits excited by neighboring cores as well (Levison et al. 2010).

4. PEBBLE ACCRETION

The observed presence of large amounts of pebbles in protoplanetary disks, as well as the theoretical and experimental understanding that pebble sizes are the natural outcome of coagulation, is strong motivation to consider pebbles, rather than planetesimals, as the fundamental building blocks of planets. Early core accretion studies did report evidence of increased accretion rates of small planetesimals due to drag, but mainly in the context of planetesimal fragments of several meters in sizes or larger (Weidenschilling & Davis 1985, Kary et al. 1993). The first simulations that showed very high accretion rates of centimeter-sized pebbles, motivated by observations of pebbles in protoplanetary disks, were presented by Johansen & Lacerda (2010). They performed hydrodynamical simulations of large planetesimals submerged in an "ocean" of pebbles and observed that the pebble component was accreted very rapidly onto the planetesimals. Ormel & Klahr (2010) analytically derived the growth rates of protoplanets accreting pebbles of different sizes, and Lambrechts & Johansen (2012) quantified the effect of pebble accretion on reducing the growth timescales of cores to below the typical lifetimes of protoplanetary disks, even for planets at orbital distances out to 100 AU.

The high accretion rates of pebbles arise from the drag force exerted on the particles by the gas in the protoplanetary disk. Kinetic energy dissipation by gas drag fundamentally changes the scattering process of a pebble passing by a growing core. The characteristic interaction radius $R_{\rm g}$ of a planetesimal or protoplanet of mass M that exerts gravity on a particle passing at the relative speed δv is simply

$$R_{\rm g} = \frac{GM}{\delta v^2}. \quad (21)$$

This gravitational radius can be equated with either the Bondi radius $R_{\rm B}$, if the relative speed is dominated by the sub-Keplerian speed Δv of the particles (following the naming convention in

Lambrechts & Johansen 2012), or with the Hill radius R_H, if the relative speed is dominated by the Hill speed $v_H = \Omega R_H$. The transition mass between those two regimes is found by equating Δv with ΩR_H to obtain

$$M_t = \sqrt{\frac{1}{3}}\frac{\Delta v^3}{G\Omega} = 2.2 \times 10^{-3}\,M_\oplus \left(\frac{r}{5\,\mathrm{AU}}\right)^{3/2}\left(\frac{\Delta v}{30\,\mathrm{m\,s^{-1}}}\right)^3. \quad (22)$$

Bondi accretion: pebble accretion with approach speed set by the sub-Keplerian speed Δv

Hill accretion: pebble accretion with approach speed set by the Hill speed $v_H = \Omega R_H$

Here we have normalized to a sub-Keplerian speed of 30 m s^{-1}, but the actual value of the radial pressure support (which sets the sub-Keplerian speed) varies with distance from the star (Chiang & Youdin 2010, Bitsch et al. 2015a). The transition mass is typically somewhere between the mass of Ceres ($M_{Ceres} = 1.5 \times 10^{-4}\,M_\oplus$) and the Moon ($M_{Moon} = 1.2 \times 10^{-2}\,M_\oplus$). Broadly speaking, planetesimals accrete pebbles in the Bondi regime (or drift regime), and protoplanets accrete in the Hill regime (or shear regime). The corresponding transition radius is

$$R_t = 1,160\,\mathrm{km}\left(\frac{r}{5\,\mathrm{AU}}\right)^{1/2}\left(\frac{\Delta v}{30\,\mathrm{m\,s^{-1}}}\right)\left(\frac{\rho_\bullet}{2\times 10^3\,\mathrm{kg\,m^{-3}}}\right)^{-1/3}. \quad (23)$$

We now discuss in detail the two regimes of pebble accretion plus the additional geometric regime that is relevant for small planetesimals.

4.1. Bondi (Drift) Accretion

In the Bondi regime, pebbles are transported past the growing planetesimal by the azimuthal and radial drift of the pebbles. For small pebbles with Stokes number less than 0.1, the azimuthal drift is dominant, and the pebbles embedded in the gas move approximately with the sub-Keplerian speed Δv. The characteristic radius for pebble accretion is the Bondi radius

$$R_B = \frac{GM}{\Delta v^2}. \quad (24)$$

The accretion radius for pebble accretion is set by the friction time of the pebbles t_f relative to the characteristic timescale to pass the core, $t_B = R_B/\Delta v$. In **Figure 1** we show the trajectories of pebbles approaching a planetesimal with the sub-Keplerian flow. Very large pebbles, with friction times of $100\,t_B$ (*blue trajectories*) are scattered by the protoplanet because of the relatively weak drag. The optimally accreted pebbles have a friction time equal to t_B (*red lines*) and are accreted from within most of the Bondi radius. Strongly coupled particles, with friction time shorter than t_B, are accreted from smaller impact parameters only.

4.2. Hill (Shear) Accretion

Above the transition mass, the sub-Keplerian speed Δv is lower than the Hill speed $v_H = \Omega R_H$. Pebbles approach the protoplanet with the Keplerian shear flow: from interior, faster orbits and exterior, slower orbits. The characteristic timescale to pass the Hill radius is $t_H = \Omega^{-1}$, independent of the mass of the protoplanet. Therefore, the accretion radius of the protoplanet is determined directly by the Stokes number of the pebbles. **Figure 2** shows trajectories of pebbles in the Hill regime. Again we see that the weakly coupled pebbles are scattered like planetesimals (*blue trajectories*), whereas the optimally and strongly coupled pebbles (*red*, *orange*) are accreted from most of the Hill radius.

The Coriolis force plays an important role in the dynamics of pebbles in the Hill regime. Even optimally coupled pebbles enter horseshoe orbits when incoming at low impact parameters. The pebbles that collide with the core inherit the rotation direction of the protoplanetary disk and impart a net prograde angular momentum to the protoplanet. This effect was observed to be much stronger when simulations include the back-reaction friction force from the particles

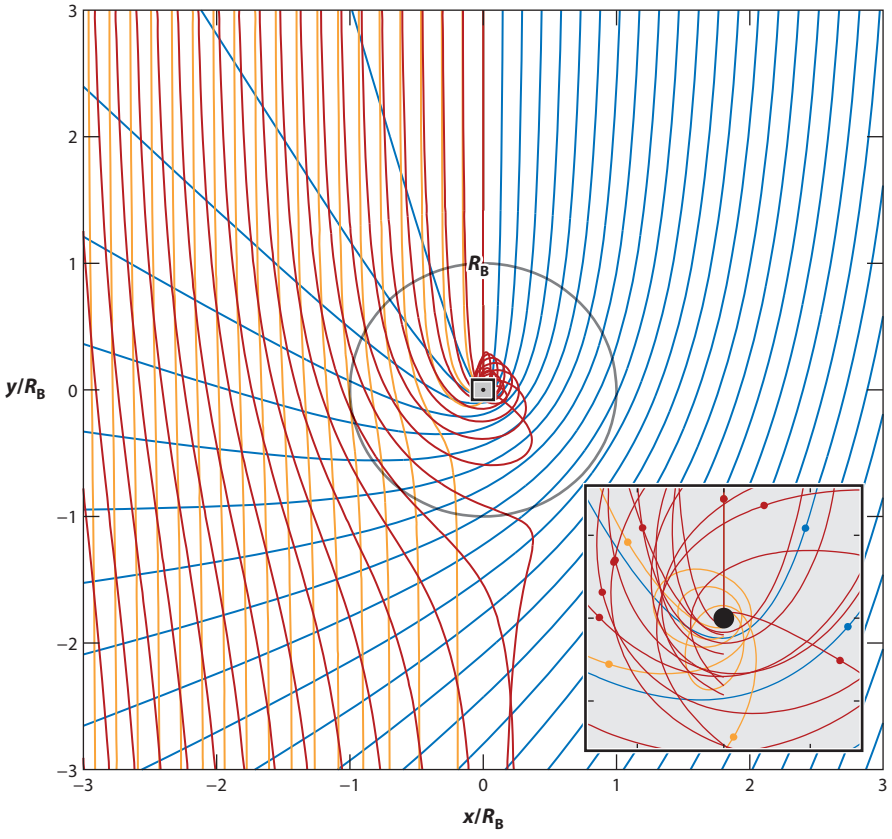

Figure 1

Accretion of pebbles in the Bondi regime. Axes are normalized by the Bondi radius, R_B. The pebbles enter from above with the sub-Keplerian speed Δv. The blue trajectories show pebbles with friction times much longer than the characteristic timescale to pass the planetesimal, the red show the optimal friction time (with friction time, t_f, relative to the timescale to pass the Bondi radius, t_B, equal to 1), and the orange trajectories show strongly coupled pebbles ($t_f/t_B = 0.1$). The inset demonstrates how the weakly coupled pebbles are scattered by the planetesimal, whereas the marginally and strongly coupled pebbles enter complex decaying orbits around the planetesimal. Colored dots mark incoming trajectories.

onto the gas, as the incoming pebbles force the gas to rotate around the protoplanet and hence the ability of the gas to remove angular momentum from the pebbles is diminished (Johansen & Lacerda 2010).

4.3. Geometric Regime

The third regime of pebble accretion, the geometric regime, is relevant when the Bondi radius is smaller than the physical radius of the planetesimal. This case was considered by Johansen et al. (2015) and Visser & Ormel (2016). The transition between the geometric and the Bondi regimes occurs when the mass is

$$M_{\rm geo} = \frac{\Delta v^3}{[(4\pi/3)G^3\rho_\bullet]^{1/2}} = 9.1\times10^{-8}{\rm M}_\oplus\left(\frac{\Delta v}{30\,{\rm m\,s^{-1}}}\right)^3\left(\frac{\rho_\bullet}{2\times10^3\,{\rm kg\,m^{-3}}}\right)^{-1/2}. \quad (25)$$

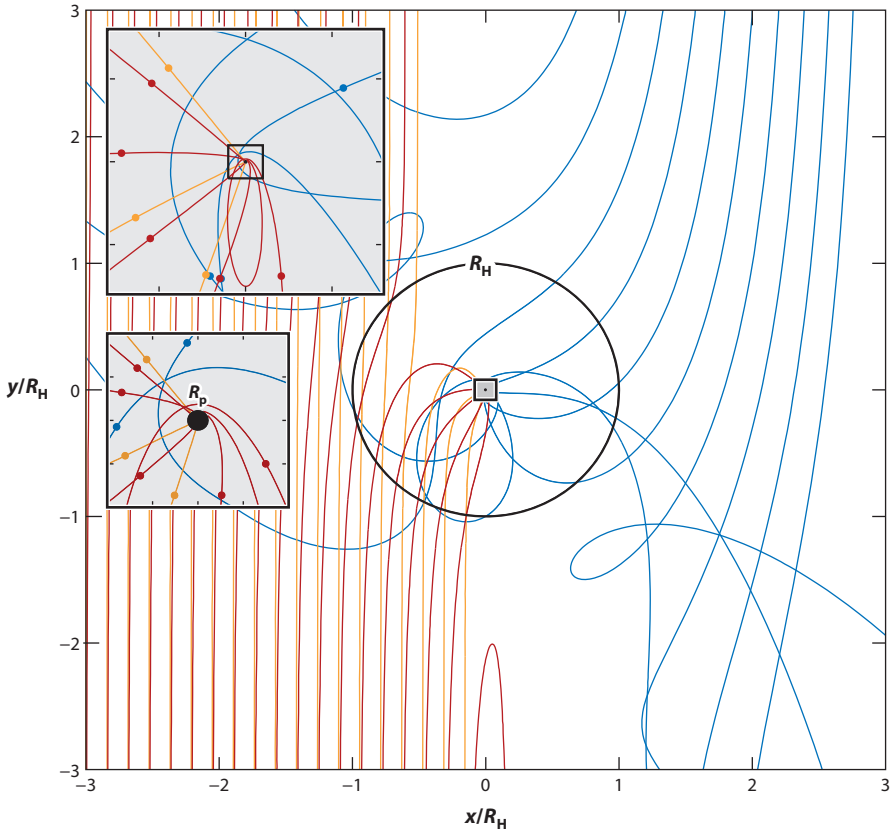

Figure 2

Accretion of pebbles in the Hill regime. Axes are normalized by the Hill radius, R_H. Very large pebbles that couple to the gas on a timescale much longer than the orbital timescale (*blue lines*) are scattered by the protoplanet, but optimally coupled pebbles with Stokes number $\mathrm{St} = 1$ (*red lines*) and strongly coupled pebbles with $\mathrm{St} = 0.1$ (*orange lines*) are accreted from most of the Hill radius. The protoplanet radius R_p is just 0.001 times its Hill radius; hence, we show insets at two different scales.

The corresponding transition radius is

$$R_{\mathrm{geo}} = 40\,\mathrm{km}\left(\frac{\Delta v}{30\,\mathrm{m\,s^{-1}}}\right)\left(\frac{\rho_\bullet}{2\times 10^3\,\mathrm{kg\,m^{-3}}}\right)^{-1/2}. \tag{26}$$

The geometric regime is characterized by the timescale to pass over the size of the planetesimal, $R/\Delta v$. Large pebbles with a friction time longer than the passing time are accreted geometrically. The pebbles arrive at the surface with a speed that is much higher than the escape speed of the planetesimal; hence, they may escape the planetesimal following an elastic collision. Energy dissipation in the collision nevertheless facilitates accretion. The optimally coupled pebble is accreted even in the absence of energy dissipation in the collision, as the gas drag dissipates kinetic energy. Strongly coupled pebbles are transported around the planetesimal by gas drag, yielding an accretion efficiency that depends on both friction time and the detailed gas flow pattern (Visser & Ormel 2016). The efficiency of pebble accretion in the geometric regime is low, as the planetesimal has a maximal capture radius equal to its own size. The geometric regime is a bottleneck in the growth

of protoplanets by pebble accretion (Guillot et al. 2014, Visser & Ormel 2016), so mutual planetesimal collisions are necessary to drive the growth of such small planetesimals (see Section 5.4).

Strong coupling branch: accretion of pebbles with friction times much shorter than the characteristic timescale to pass the protoplanet

Weak coupling branch: accretion of pebbles with friction times much longer than the characteristic timescale to pass the protoplanet

4.4. Analytical Pebble Accretion Rates

The accretion rates of pebbles depend sensitively on the friction time of the pebbles. The most general expressions for the accretion rates in 2D and 3D can be written as

$$\dot{M}_{2D} = 2 R_{acc} \Sigma_p \delta v, \tag{27}$$

$$\dot{M}_{3D} = \pi R_{acc}^2 \rho_p \delta v. \tag{28}$$

Here, R_{acc} is the accretion radius, and Σ_p and ρ_p are the pebble column density and midplane density, respectively. The approach speed is defined as $\delta v \equiv \Delta v + \Omega R_{acc}$. The accretion radius R_{acc} contains all the dependence on the friction time. Lambrechts & Johansen (2012) used simple scaling arguments to derive the friction time dependence in the Bondi and Hill limits. Here, we generalize this to a single expression. The accretion criterion is that the pebble must be able to change direction significantly on a timescale that is shorter than the friction time. This yields the accretion criterion

$$\tau_f = \frac{\xi_B \Delta v + \xi_H \Omega \hat{R}_{acc}}{GM/\hat{R}_{acc}^2}. \tag{29}$$

We have used $\hat{R}_{acc}$ here to mark that this criterion is valid in the limit of strong coupling (low friction time). The parameters ξ_B and ξ_H give two degrees of freedom to match the resulting accretion radius in the limits of Bondi accretion ($\Delta v \gg \Omega R_H$) and Hill accretion ($\Delta v \ll \Omega R_H$). Equation 29 describes a third-order polynomial in $\hat{R}_{acc}$ with no simple analytical solution, but an iterative Newton-Raphson procedure can be used to find $\hat{R}_{acc}$. Using $\xi_B = \xi_H = 0.25$ yields good fits to the limiting behaviors found by Ormel & Klahr (2010) and Lambrechts & Johansen (2012),

$$\hat{R}_{acc} = \left(\frac{4\tau_f}{t_B}\right)^{1/2} R_B \qquad \text{(Bondi limit) and} \tag{30}$$

$$\hat{R}_{acc} = \left(\frac{\Omega\tau_f}{0.1}\right)^{1/3} R_H \qquad \text{(Hill limit).} \tag{31}$$

Note that the accretion rate in the Hill limit is $\dot{M}_{2D} \propto (\Omega\tau_f)^{2/3}$ in 2D and $\dot{M}_{3D} \propto (\Omega\tau_f)$ in 3D because the approach speed δv contains another linear dependence on the accretion radius (Lambrechts & Johansen 2014 , Morbidelli et al. 2015).

Pebble accretion nevertheless becomes inefficient for friction times that are longer than the time to pass the protoplanet. This limit is not taken into account in the expressions above, which are only valid for the strong coupling branch. There is no known analytical solution to the weak coupling branch. Ormel & Klahr (2010) proposed to multiply the strong coupling expression by an exponential term with two parameters χ and γ,

$$R_{acc} = \hat{R}_{acc} \exp[-\chi(\tau_f/t_p)^\gamma]. \tag{32}$$

Here, the characteristic passing timescale is $t_p = GM/(\Delta v + \Omega R_H)^3$. Ormel & Klahr (2010) demonstrated that $\chi = 0.4$ and $\gamma = 0.65$ provide good fits to the weak coupling branch. Gravitational focusing (Equation 13) eventually comes to dominate the accretion rate for very weakly coupled particles.

We now express the scaling of the pebble accretion rates with disk properties in the Bondi and Hill limits. The fastest accretion rate on the 3D Bondi branch occurs for pebbles with friction time $\tau_{\rm f} = t_{\rm B}$. The accretion rate comes out as

$$\dot{M}_{\rm B,3D} = 8.4 \times 10^{-3}\,{\rm M}_\oplus\,{\rm Myr}^{-1}\,f_{\rm p} \times \left(\frac{M}{10^{-4}{\rm M}_\oplus}\right)^{2} \left(\frac{\Delta v}{30\,{\rm m\,s}^{-1}}\right)^{-3} \left(\frac{H_{\rm p}/H}{0.1}\right)^{-1} \left(\frac{H/r}{0.05}\right)^{-1} \left(\frac{r}{5\,{\rm AU}}\right)^{-2}. \quad (33)$$

For the Hill branch, we focus on 2D growth and set $\Omega\tau_{\rm f} = 0.1$ to yield the accretion rate

$$\dot{M}_{\rm H,2D} = 210\,{\rm M}_\oplus\,{\rm Myr}^{-1}\,f_{\rm p} \left(\frac{M}{{\rm M}_\oplus}\right)^{2/3} \left(\frac{r}{5\,{\rm AU}}\right)^{-0.5}. \quad (34)$$

The scaling with M describes orderly growth on the Hill branch and runaway growth on the Bondi branch. The runaway timescale on the Bondi branch is

$$\tau_{\rm run} = \frac{M}{\dot{M}_{\rm B,3D}} = 1.2 \times 10^{-2}\,{\rm Myr}\,f_{\rm p}^{-1} \times \left(\frac{M}{10^{-4}{\rm M}_\oplus}\right)^{-1} \left(\frac{\Delta v}{30\,{\rm m\,s}^{-1}}\right)^{3} \left(\frac{H_{\rm p}/H}{0.1}\right) \left(\frac{H/r}{0.05}\right) \left(\frac{r}{5\,{\rm AU}}\right)^{2}. \quad (35)$$

Ceres-mass planetesimals can grow out to 10 AU within a million years. Growth at 100 AU requires starting with Moon-mass protoplanets or higher disk masses (higher $f_{\rm p}$).

4.5. Transition from Bondi to Hill Accretion

The accretion rate expressions presented in the previous subsection have been tested and calibrated in the limits of Bondi accretion (small planetesimals) and Hill accretion (large protoplanets). Here, we compare the measured accretion rate of a planetesimal that grows to a full planet by pebble accretion to the analytical expressions.

We integrate a high number of pebble trajectories for a range of protoplanet masses from $10^{-6}\,{\rm M}_\oplus$ to $10^{2}\,{\rm M}_\oplus$ placed at $r = 5$ AU. **Figure 3** shows the impact parameter range (radial displacement relative to the protoplanet) of accreted pebbles, as a function of the protoplanet mass. We have normalized the impact parameter with the size of the protoplanet, so that the Bondi radius (*red line*) appears as a curve proportional to $M^{2/3}$ and the Hill radius (*orange lines*) appears as a constant curve. The radial drift of the pebbles pushes the accretion regions to exterior orbits, but the impact parameter range still follows approximately the size of the Bondi radius until the transition mass is reached. Beyond the transition mass, two accretion regions appear, one for interior, faster orbits and one for exterior, slower orbits. The regions eventually merge for protoplanet masses beyond 10 Earth masses.

Figure 3 illustrates how complicated pebble accretion appears when looking at individual pebble trajectories. However, **Figure 4** shows that the accretion rate is relatively easy to understand. We have assigned a mass density to each of the pebble trajectories that are successfully accreted by the protoplanet and have summed them to obtain the accretion rate. The accretion rate follows marginally and weakly coupled Bondi accretion very well below the transition mass (*red line*) and the Hill regime scaling $\dot{M} \propto M^{2/3}$ above the transition mass (*orange line*). Gravitational focusing of pebbles dominates the accretion rate for the smallest planetesimals below $10^{-4}{\rm M}_\oplus$ because the 10-cm-sized pebbles considered here are too weakly coupled to the gas to undergo Bondi accretion at those planetesimal masses.

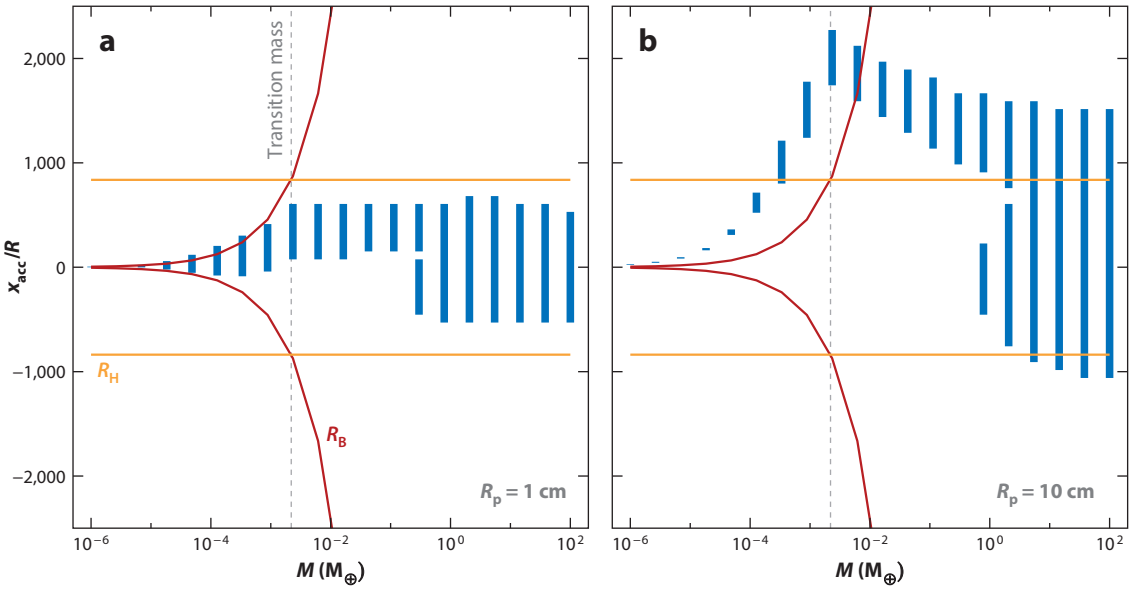

Figure 3

The range of impact parameters x_{acc} of pebbles that are accreted by a growing planet located at $r = 5$ AU as a function of the planet mass M. The impact parameter is normalized by the planetary size R. The panels consider pebbles of size (*a*) $R_p = 1$ cm and (*b*) $R_p = 10$ cm. The accretion region initially follows the Bondi radius R_B (*red curves*), but above the transition mass (*gray dotted line*), the Hill radius R_H (*orange curve*) is followed closely. There is a preference for accretion from exterior orbits owing to the radial drift of the pebbles.

Figure 4*b* shows the integrated mass of the protoplanet as a function of time. The long time spent on the Bondi accretion branch acts as a "ketchup" bottleneck in that it has very slow growth below the transition mass but then enters a runaway accretion near the transition mass. Therefore, the initial planetesimal mass is crucial for determining the timescale it takes to grow up to a core mass that can accrete gas. Starting at 10^{-4} $M_\oplus$, it takes just 0.1 Myr, and the timescale extends to more than 2 Myr when starting at 2×10^{-6} $M_\oplus$.

4.6. The Effect of Eccentricity and Inclination

The relative speed between a protoplanet on an eccentric and inclined orbit and pebbles moving with the sub-Keplerian speed Δv can be written as a function of time t as

$$v_{rel} = \sqrt{[v_e \cos(\Omega t)]^2 + [-(1/2)v_e \sin(\Omega t) + \Delta v]^2 + [v_i \cos(\Omega t)]^2}. \quad (36)$$

Here, $v_e = ev_K$ and $v_i = iv_K$ are the eccentricity and inclination speeds of the orbit, and v_K is the Keplerian speed. The relative speed is lowest at aphelion ($\Omega t = \pi/2$) and highest at perihelion ($\Omega t = 3\pi/2$). Because the Bondi radius scales as $R_B \propto 1/v_{rel}^2$, the eccentric motion strongly affects the accretion rate. The inclination has the further effect of lifting protoplanets to orbits that are detached from the midplane layer of pebbles. The maximum height of the protoplanet over the midplane reaches $z_{max} = iv_{K,0}/\Omega = ir$. Here, $v_{K,0}$ is the Keplerian speed at the center of the coordinate frame. For a midplane scale-height of H_p, the detachment from the midplane happens at $i \sim H_p/r$. The streaming instability results in $H_p/H \sim 0.01$ for a wide range of particle sizes, and hence, the limiting inclination becomes $i \sim 0.01H/r \sim 0.001$. Levison et al. (2015a)

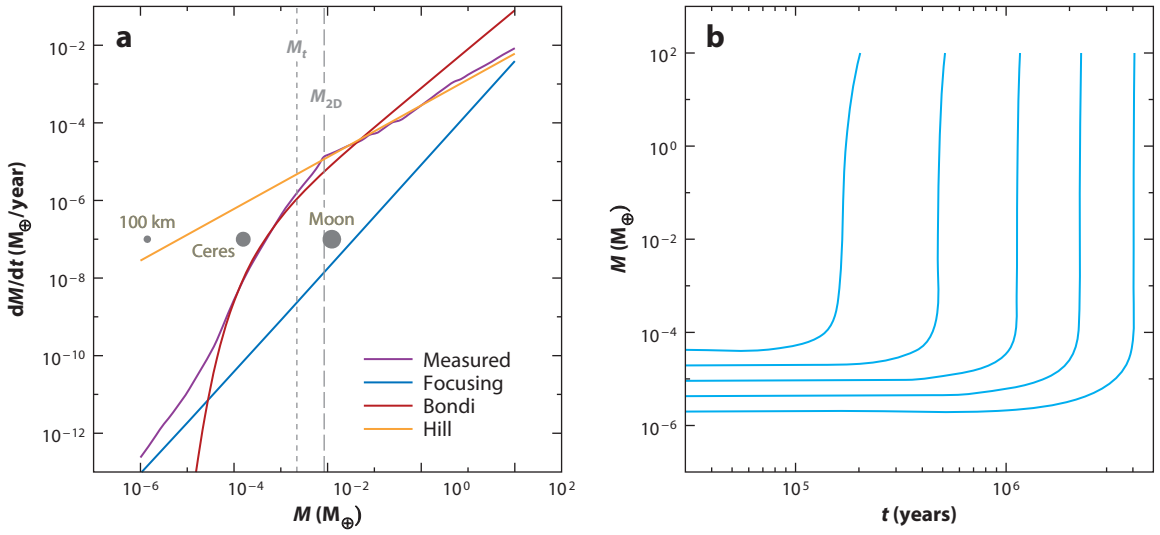

Figure 4

(*a*) The measured accretion rate of a protoplanet accreting pebbles of 10 cm in size as a function of its mass M and (*b*) the integrated mass as a function of time starting at different planetesimal masses. We mark the transition from 3D to 2D pebble accretion (M_{2D}), as well as the transition mass (M_t), which are quite close in value. The accretion rate is measured from the numerical integrations of pebble trajectories presented in **Figure 3**. Despite the complexity of the actual pebble trajectories, the accretion rate follows the scaling in the gravitational focusing regime (*blue*), Bondi regime (*red*), and Hill regime (*orange*) well. Panel *b* shows that the protoplanet spends most of its time on the focusing and Bondi branches. The total growth time of the planet is therefore determined by the initial planetesimal mass.

considered the effect of the eccentricity and inclinations of protoplanets competing for pebbles in an N-body simulation that evolves the orbits of the bodies self-consistently. They found that the four largest protoplanets lift their smaller counterparts out of the midplane layer and quench their ability to accrete pebbles. This way, pebble accretion leads naturally to the formation of a low number of giant planets and avoids entering an oligarchic growth stage where the pebbles are spread over a myriad of protoplanets (Kretke & Levison 2014). Other N-body pebble accretion codes are currently under development (e.g., Chambers 2016). Inclusion of N-body effects in pebble accretion simulations is clearly an important step toward forming fully self-consistent planetary systems.

4.7. Halting Pebble Accretion

Core growth by pebble accretion is fueled by pebbles drifting in from outer orbits. If this supply is interrupted, then core growth comes to a standstill. Massive cores gravitationally perturb the gas disk, and in this way they carve a shallow gap. The edges act as pressure bumps, where the gas orbits at Keplerian speed, thereby halting the radial drift of pebbles to the core. The first-order perturbation on the gas velocity caused by the gravity of the core can be approximated as

$$\Delta u_y \sim \frac{GM}{rH\Omega}, \tag{37}$$

at a radial distance of one gas scale-height H from the core (Muto & Inutsuka 2009). We can balance this perturbation with the sub-Keplerian flow of the gas

$$\Delta v \sim \left(\frac{H}{r}\right)^2 \frac{\partial \ln P}{\partial \ln r} v_{\rm K}, \tag{38}$$

in order to identify the pebble isolation mass

$$M_{\rm iso} \sim \left(\frac{H}{r}\right)^3 \frac{\partial \ln P}{\partial \ln r} M_\star \approx 20 \left(\frac{H/r}{0.05}\right)^3 {\rm M}_\oplus. \tag{39}$$

Here, $M_\star$ is the stellar mass, and the prefactor in the last expression (Equation 39) comes from numerical experiments (Lambrechts et al. 2014). In a flared disk, where the aspect ratio H/r increases, the pebble isolation mass increases with orbital radius, and isolation becomes harder to obtain. There are two major implications of this pebble isolation mass (Lambrechts et al. 2014). First, if one core reaches pebble isolation, it cuts the flow of pebbles to all interior protoplanets and stifles their growth. Protoplanets just below the isolation mass filter only approximately 10% of the drifting pebbles (Morbidelli & Nesvorny 2012, Lambrechts & Johansen 2014), and even a whole belt of small planetesimals has only a minor combined filtering fraction (Guillot et al. 2014). Second, when a core reaches isolation, it starts the process of attracting a gaseous envelope. This is discussed in more detail in Section 5. Morbidelli et al. (2015) proposed a scenario in which the cores of the giant planets in the Solar System cut off the flow of pebbles to interior orbits, preventing the growth of terrestrial protoplanets more massive than Mars. This would explain the dichotomy between small terrestrial protoplanets and large giant planet cores in wider orbits.

5. PLANETARY GROWTH TRACKS

Planets undergo migration while they grow by accreting pebbles and planetesimals. Planetary migration has been a long-standing challenge for traditional planet formation scenarios that relied solely on planetesimal accretion, as protoplanets will consistently migrate into the inner regions of the protoplanetary disk while they grow (Coleman & Nelson 2016). Pebble accretion overcomes this issue in two ways. First, growth rates by pebble accretion are high enough to form the cores of the giant planets in a million years or less. This way, protoplanets undergo less migration while growing. Second, the accretion rate by pebble accretion only decreases with semimajor axis as $r^{-0.5}$ (Equation 34). Hence, accretion rates are high even out to tens of AU from the central star. This is in contrast to planetesimal accretion, which falls as $r^{-1.5}$ (Equation 19). Pebble accretion thus allows the cores of giant planets to start growing well beyond their final parking position, and this way, they can undergo substantial migration while still being consistent with the formation of giant planets in cold orbits.

In this section we review the physics involved in integrating planetary growth tracks and present a simple model to calculate example growth tracks of hot and cold gas giants, ice giants, wide-orbit planets, and super-Earths. The underlying protoplanetary disk model has a strong influence on these growth tracks. These model dependencies are currently under active investigation (Lambrechts & Johansen 2014 , Bitsch et al. 2015b, Bitsch & Johansen 2016, Chambers 2016, Ida et al. 2016).

5.1. Planetary Migration

Low-mass planetary cores migrate in response to the gravitational torques from the wakes excited in the gas. We consider a Type I migration rate $v_r^{(\rm I)}$ that follows Tanaka et al. (2002),

$$v_r^{(\rm I)} = -c \frac{M}{M_\star} \frac{\Sigma_{\rm g} r^2}{M_\star} \left(\frac{H}{r}\right)^{-2} v_{\rm K}. \tag{40}$$

Here, c is a dimensionless parameter that we set for simplicity to 2.4, M is the planetary mass, and $M_\star$ is the mass of the central star. We ignore all other aspects of Type I migration here, for example, outward migration due to the corotation torque (Paardekooper et al. 2011) and the so-called heating torque caused by the accretional heating of the protoplanet (Benítez-Llambay et al. 2015). These are clearly important effects that can affect the growth tracks of planets (as demonstrated by Bitsch & Johansen 2016), but Bitsch et al. (2015b) showed that the overall architecture of planetary systems is set by the basic Type I migration.

Disk parameters for giant-planet model:
$f_\mathrm{g} = 0.2$
$f_\mathrm{p} = 0.4$
$f_\mathrm{pla} = 0.2$
$H/r = 0.04$
$H_\mathrm{p}/H = 0.1$
$\Delta v = 30\ \mathrm{m\ s^{-1}}$
$\mathrm{St} = 0.2$

Massive planets open a gap in the disk and undergo Type II migration. We set the radial speed $v_r^{(\mathrm{II})}$ of a planet undergoing Type II migration to be

$$v_r^{(\mathrm{II})} = \frac{r^2}{\nu} \min\left(1, \frac{4\pi \Sigma_\mathrm{g} r^2}{M}\right). \tag{41}$$

Here, r^2/ν is the viscous accretion speed of the gas, with the turbulent viscosity $\nu = \alpha c_\mathrm{s} H$. Multiplication by the min function reduces the migration rate of massive planets that dominate the mass local budget of the disk (Baruteau et al. 2014). The transition between Type I and Type II migration can be calculated using the approach of Crida & Morbidelli (2007); we follow here the procedure described by Bitsch et al. (2015b).

5.2. Accretion of Pebbles, Planetesimals, and Gas

The pebble accretion expressions are derived and tested in Section 4.4. We use Equations 27 and 28 to calculate the mass accretion rates in 2D and 3D, depending on the ratio of the accretion radius R_acc to the scale-height of the pebble midplane layer H_p. The strong coupling accretion radius is found from Equation 29 by solving the condition

$$\Phi(\hat{R}_\mathrm{acc}) = \tau_\mathrm{f} - \frac{0.25(\Delta v + \Omega \hat{R}_\mathrm{acc})}{GM/\hat{R}_\mathrm{acc}^2} = 0. \tag{42}$$

We use an iterative Newton-Raphson solver. This expression is finally multiplied by the weak coupling branch found in Equation 32. For the planetesimal accretion rate, we use Equation 17 with $\zeta = 2$ to yield a planetesimal accretion rate that is close to the maximum for the best comparison with the pebble accretion rate.

The gas envelope starts to contract after the core reaches pebble isolation mass (Equation 39). Initially, the contraction is slow, as the gravity is dominated by the mass of the solid core (Piso & Youdin 2014). This contraction continues until the envelope mass $\mathrm{M}_\oplus$ is equal to the core mass M_c. After that the self-gravity of the envelope leads to accretion of gas from the disk (Machida et al. 2010). We use here the equations for gas accretion that can be found in section 2.3 of Bitsch et al. (2015b).

5.3. Growth Tracks of Gas Giants and Ice Giants

The formation of a giant planet requires the accumulation of a massive core of at least several Earth masses. The composition of ice giants is a particular challenge (Helled & Bodenheimer 2014), as their large cores need to form at wide orbits but should not enter a stage of runaway gas accretion. For the growth tracks of gas giants and ice giants, we choose the parameters listed in the margin note. These conditions are relevant in the late stages of the evolution of a protoplanetary disk in the 10–30 AU region (Bitsch et al. 2015a). The growth tracks are shown in **Figure 5**. We find that growth from the starting mass $10^{-2}\mathrm{M}_\oplus$ to fully formed planets takes approximately 1 Myr. The preceding 2–4 Myr, depending on the total disk lifetime, would then be spent mainly in the growth from planetesimal sizes to protoplanets (see Section 5.4).

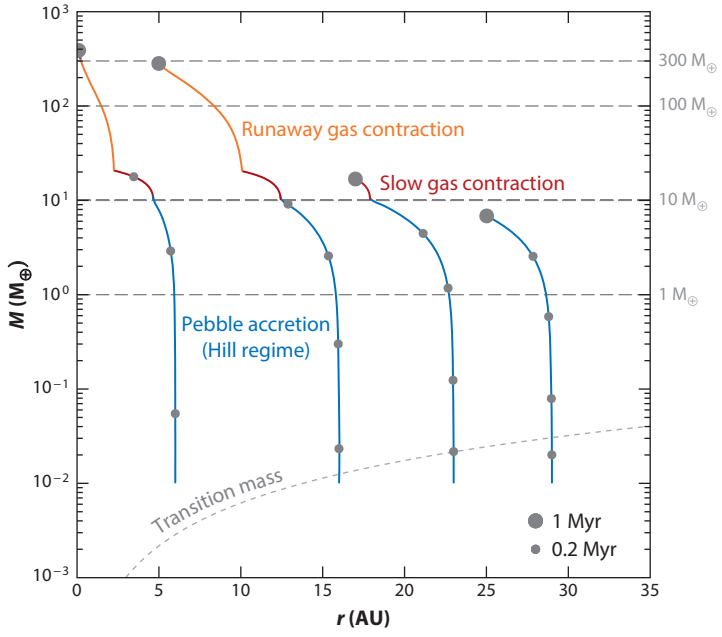

Figure 5

Growth tracks for (from the left) a hot gas giant, a Jupiter-analogue cold gas giant, an ice giant with an envelope and an envelope-free ice giant. The large dots mark the end of the simulation and 1-Myr intervals backward in time, and the smaller dots mark intervals of 0.2 Myr. The hot gas giant forms its core (*blue curve*) between 6 AU and 5 AU and subsequently undergoes migration to 0.1 AU while accreting more than one Jupiter mass of gas (*red and orange curves*). The cold ice giant must start further out, at 16 AU, to end in a Jupiter-like orbit. The two ice giants form even further out. The innermost, starting at 23 AU, reaches the pebble isolation mass of 10 $M_\oplus$ and enters a phase of envelope contraction that is terminated by the dissipation of the protoplanetary disk, whereas the outermost ice giant never reaches pebble isolation mass and hence acquires no gaseous envelope.

Figure 5 illustrates the important role of migration defining the growth tracks of giant planets. The protoplanet starting at 6 AU migrates to form a hot gas giant at 0.1 AU (we arbitrarily stop both growth and migration at the assumed inner disk edge at 0.1 AU). Forming a Jupiter analogue at 5 AU requires the protoplanet to start growing at 16 AU. The protoplanet migrates 3 AU while accreting pebbles and then another 8 AU while accreting gas. The protoplanets starting at 23 AU and 30 AU never reach the gas accretion phase. This is because we have forced these protoplanets to stop at 17 AU and 25 AU, under the assumption that photoevaporation eventually dissipates the protoplanetary disk. The protoplanet starting at 23 AU grows to an ice giant with a significant gaseous envelope but never undergoes gas accretion from the disk. The protoplanet starting at 30 AU, in contrast, has only grown to 7$M_\oplus$, below the pebble isolation mass, when it arrives at its final position at 25 AU.

5.4. Growth to Transition Mass

The growth tracks presented in **Figure 5** all arbitrarily start at $10^{-2}M_\oplus$. However, this mass is orders of magnitude higher than the birth masses of planetesimals formed by the streaming instability. These planetesimals have characteristic masses between $10^{-6}M_\oplus$ (100-km-radius asteroid) and $10^{-4}M_\oplus$ (Ceres) (see Johansen et al. 2015, Simon et al. 2016). The Bondi accretion of pebbles

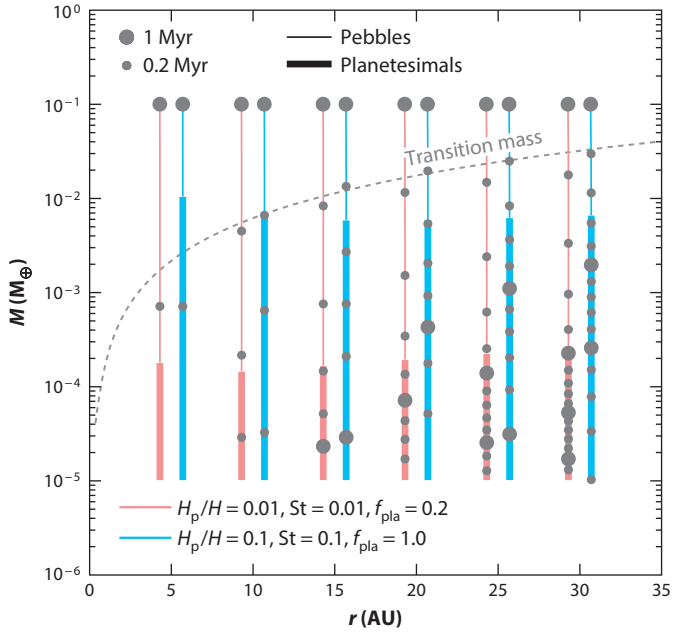

Figure 6

Growth tracks of planetesimals starting at $10^{-5}M_\oplus$. We show two models, one that is pebble driven (*red*) with a dense pebble midplane layer of small pebbles and another that is planetesimal driven (*blue*) with a planetesimal population of nominal column density. Both models allow growth to 0.1 $M_\oplus$ within a few million years out to 30 AU, although the pebble model struggles with long timescales at large distances. The model parameters indicated at the bottom are the ratio of the pebble midplane layer thickness to the gas scale-height, H_p/H, the pebble Stokes number St, and the ratio of the planetesimal column density to its nominal 1% value of the gas column density, f_{pla}.

Disk parameters for pebble model: like giant-planet model but with $H_p/H = 0.01$ and St = 0.01

Disk parameters for planetesimal model: like giant-planet model but with $f_{pla} = 1.0$

is very efficient near the transition mass to Hill accretion. Newly born planetesimals nevertheless have such small masses than even Bondi accretion is inefficient, owing to its squared dependence on the mass as well as the requirement to accrete pebbles that couple to the gas on the Bondi timescale. The latter means that even small pebbles of St $\sim$ 0.1 do not lead to any appreciable growth of planetesimals. **Figure 6** demonstrates the growth from planetesimal masses ($10^{-5}M_\oplus$) to protoplanets ($10^{-1}M_\oplus$). We consider two models. The pebble model employs a dense midplane layer of small pebbles with St = 0.01 that attach well to the Bondi branch. The other model, the planetesimal model, has an additional population of planetesimals of nominal column density. Growth to protoplanet masses in **Figure 6** is possible for both the pebble model and the planetesimal model. The timescales for both planetesimal accretion and Bondi accretion are increasingly longer the further out the planetesimal starts. However, growth is achievable within a few million years out to 30 AU for both models. Planetesimal accretion clearly plays an important role in forming protoplanets that can subsequently undergo rapid pebble accretion.

5.5. Growth Tracks of Wide-Orbit Exoplanets

Direct imaging surveys of exoplanets around nearby, young stars have yielded several systems of wide-orbit gas giants. The clearest example of planet formation in wide orbits is arguably HR 8799 (Marois et al. 2008, 2010). The four known planets in this system orbit at 15, 24, 38, and 68 AU. The inner three planets have deduced masses, based on their luminosity and the uncertain age of

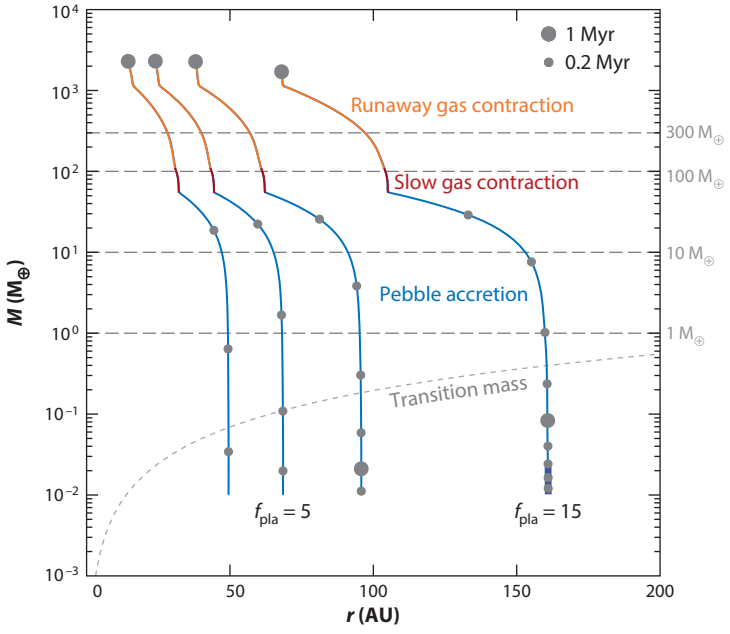

Figure 7

Growth tracks for exoplanets in wide orbits. We stop the planets here in the architecture of the observed wide-orbit system HR 8799. The three innermost planets start between 50 and 100 AU and migrate 30–60 AU during their growth. The growth timescale is still comfortably within 3 Myr for these planets. The outermost planet in the HR 8799 system is more challenging and requires boosting the planetesimal density to 15 times the nominal value, $f_{\rm pla} = 15$, to not get stuck at the starting mass where pebble accretion is not efficient. The protoplanet migrates 90 AU during its growth to end up in an orbit at 68 AU.

the system, of $M \approx 7\,M_{\rm J}$, and the outer planet is likely less massive with $M \approx 5\,M_{\rm J}$. Despite the mass of the central A star of $1.5\,M_\odot$, these planets are so close to each other to be on the verge of stability and the system likely owes its continued existence to its youth (Gotberg et al. 2016) and/or protection by resonances (Fabrycky & Murray-Clay 2010).

Wide-orbit exoplanet systems pose a challenge to planet formation because of the long formation timescales at those distances. The low planetesimal accretion rate in wide orbits gives no appreciable growth (Dodson-Robinson et al. 2009). Here we demonstrate growth tracks of wide-orbit exoplanets that form mainly by pebble accretion. We use the parameters listed in the margin note. We use a nominal column density here, to reflect that protoplanetary disks around A stars are in general more massive, so that the protoplanetary disk could have formed planetesimals in a young, massive disk with $f_{\rm g} = f_{\rm pla} = 5$ that is now a few million years later in a more evolved stage with $f_{\rm g} = 1$ but retaining $f_{\rm pla} = 5$.

Disk parameters for wide-orbit model:
$f_{\rm g} = 1.0$
$f_{\rm p} = 0.4$
$f_{\rm pla} = 5$
$H/r = 0.07$
$H_{\rm p}/H = 0.1$
$\Delta v = 30\ {\rm m\ s^{-1}}$
${\rm St} = 0.2$

The growth tracks are shown in **Figure 7**. We terminate the growth tracks at the current positions of the four planets in HR 8799. The innermost planet grows from $10^{-2} M_\oplus$ to its final mass in less than 800,000 yr, whereas it takes more than 1.2 Myr for the third planet. All planets undergo substantial migration while they grow. This is due to the low pebble accretion rates. The outermost planet is the hardest to form because it has a relatively high mass in a very wide orbit. To be consistent with Type I migration, the planets must form at 160 AU, and a large planetesimal column density $f_{\rm pla} = 15$ is required to avoid getting stuck in the growth from $10^{-2} M_\oplus$ to $10^{-1} M_\oplus$.

Forming the outer planet of the HR 8799 system is clearly at the limit of what can be achieved by pebble accretion.

Disk parameters for super-Earth model:
$f_g = 0.2$
$f_p = 0.4$
$f_{pla} = 1.0$
$H/r = 0.03$
$H_p/H = 0.1$
$\Delta v = 30$ m s^{-1}
St $= 0.01$

5.6. Growth Tracks of Super-Earths

Ground-based radial velocity surveys, and particularly the ongoing transit survey by the Kepler satellite, have demonstrated that approximately half of solar-type stars are orbited by super-Earths (or mini-Neptunes) of radii less than 4 $R_\oplus$ in orbits within approximately 0.3 AU (Mayor et al. 2011, Fressin et al. 2013). The total mass of solids in close-in super-Earth systems such as the sextuple Kepler-11 (Lissauer et al. 2011) implies a pile-up of mass in the inner regions of the protoplanetary disk. In situ formation of super-Earths in orbits close to the star thus requires a column density of solids much in excess of the minimum mass solar nebula (Chiang & Laughlin 2013). The approach of constructing a protoplanetary disk column density that permits the formation of super-Earths nevertheless ignores the role of planetary migration. Ogihara et al. (2015) demonstrated that the inclusion of Type I migration in simulations of in-situ formation of super-Earths from smaller protoplanets leads to migration of the planets to the inner edge of the disk, in a way that is inconsistent with the observed orbits of super-Earths.

Growth tracks of migrating super-Earths can be produced with planetesimal accretion alone (Coleman & Nelson 2016), owing to the high planetesimal accretion rates in the inner regions of the protoplanetary disk. However, the pebble accretion rate is also increased in those regions, and pebble accretion can be an important driver for the formation of protoplanets (Johansen et al. 2015). Bitsch & Johansen (2016) showed that the growth tracks of super-Earths forming by pebble accretion have starting locations out to a typical distance 10 AU from the host star and that the growth must start late to avoid the protoplanets growing massive enough to attract a gas envelope and form hot Jupiters. The masses and orbital distances intersect with the regions of outward Type I migration (Paardekooper et al. 2011). However, the outward migration zone depends sensitively on the assumption that the opacity makes a jump at the water ice line due to the presence of icy grains outside of this distance. Lowering the metallicity or the water contents of the protoplanetary disk makes the outward migration less relevant for super-Earth growth tracks (Bitsch & Johansen 2016).

In **Figure 8**, we present super-Earth growth tracks including pebble accretion and planetesimal accretion. We start with four planetesimals of mass 10^{-5} M$_\oplus$ in the inner parts of the protoplanetary disk, located at 0.5, 1, 2, and 4 AU. The disk aspect ratio is chosen to be $H/r = 0.03$ to reflect prevalent conditions close to the star where the stellar gravity is strong (Hayashi 1981, Bitsch et al. 2015a). This yields a pebble isolation mass of just 5 M$_\oplus$. The envelope contracts very slowly on such a small core, and the protoplanets manage to accrete only a few Earth masses of hydrogen and helium, consistent with the observed gas fractions of massive super-Earths. We also use here a smaller Stokes number St $= 0.01$ because silicate particles in the inner regions of the protoplanetary disk are less sticky than ice particles. The growth is initially driven by planetesimal accretion, but pebble accretion becomes dominant when reaching approximately 10^{-2}M$_\oplus$. The cores of the super-Earths form over a relatively short interval in semimajor axis, ranging from 0.1 AU for the planetesimal that starts at 0.5 AU to 1 AU for the outermost protoplanet starting at 4 AU.

6. OUTLOOK

This review set out to demonstrate the power of pebbles in driving planet formation. Protoplanets acquire immense growth rates when accreting pebbles, even under the relatively conservative

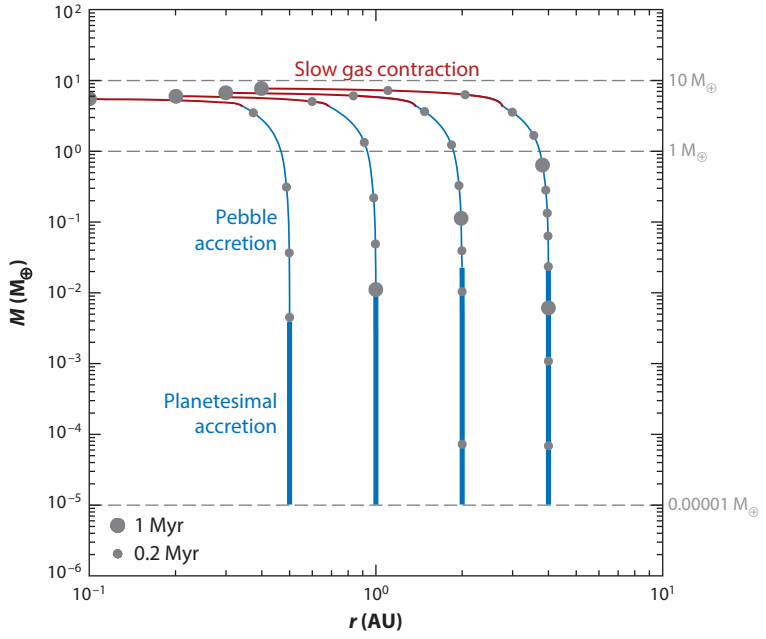

Figure 8

Growth tracks of super-Earths, including pebble accretion and planetesimal accretion. The planetesimals are started with masses of 10^{-5} $M_\oplus$ at 0.5, 1, 2, and 4 AU. The initial growth is driven by planetesimal accretion, up to a mass of 10^{-3}–10^{-2} $M_\oplus$. From that point pebble accretion becomes dominant and drives the growth up to pebble isolation at approximately 5 $M_\oplus$. This low pebble isolation mass is caused by the low value of the disk aspect ratio H/r in the inner regions of the protoplanetary disk and in turns leads to a slow contraction of the envelope that is stopped by photoevaporation. The result is a super-Earth consisting of a solid core and an envelope of a few Earth masses of hydrogen and helium.

assumptions about protoplanetary disk masses, pebble sizes, and pebble sedimentation that we have employed here. We have shown that the formation of all the major classes of planets can be understood in the pebble accretion framework and that planets undergo substantial migration while they grow. Planetary migration is no longer a bottleneck when planets grow by pebble accretion, but rather an essential aid in arriving at the observed orbital architectures of our Solar System as well as the multitude of planetary systems around other stars that are being mapped in more and more detail.

SUMMARY POINTS

1. Protoplanetary disks are excellent pebble factories. The observed populations of millimeter- to centimeter-sized pebbles are consistent with pebble growth limited by sticking and drift barriers.
2. The characteristic scale of planetesimals formed by the streaming instability is approximately 100 km, in good agreement with the observed bump at 100-km diameters in the size distribution of asteroids.

3. Planetesimals of such sizes grow initially mainly by mutual collisions.
4. Pebble accretion becomes the dominant growth mechanism starting from between approximately the mass of Ceres and the mass of the Moon.
5. Pebble accretion is halted at the pebble isolation mass of approximately 10 $M_\oplus$. The termination of accretion heat initiates the contraction of the gas envelope.
6. Large protoplanets quench pebble accretion onto their smaller cousins by exciting their orbital inclination. This way only the largest protoplanets remain attached to the pebble midplane layer, and a low number of giant planets are formed naturally.
7. In the pebble accretion framework all the major classes of gaseous planets—gas giants, ice giants and super-Earths with envelopes—undergo migration over distances comparable to their initial semimajor axis while they grow.

FUTURE ISSUES

1. Dust growth: The drift-limited solution for pebble formation gives a good match to observations of pebble sizes in protoplanetary disks (Birnstiel et al. 2012). Several aspects of dust growth are nevertheless not well understood, including the formation of fluffy ice aggregates (Okuzumi et al. 2012), condensation of volatiles near ice lines (Ros & Johansen 2013) and the role of bouncing for CO_2 and CO ice (Musiolik et al. 2016). More observations of the radial dependence of pebble sizes in protoplanetary disks, coagulation models that include volatile species, and experiments on the sticking properties of aggregates of a range of compositions will be needed to understand pebble formation better.
2. Planetesimal formation: The streaming instability requires a dust-to-gas ratio slightly above the solar value. Hence, planetesimal formation may be a local process that is triggered only in regions where the gas density is low (due to photoevaporation; e.g., Gorti et al. 2015) and/or the particle density is high (due to particle pile-ups; e.g., Youdin & Chiang 2004, Drążkowska et al. 2016). Better models for when and where planetesimals form will also require an increased understanding of the interaction between the streaming instability and the vertical shear (Nelson et al. 2013) and baroclinic (Raettig et al. 2013) instabilities that can drive turbulence in the planet-forming regions of protoplanetary disks.
3. Pebble accretion: The relative roles of pebble accretion and planetesimal accretion/giant impacts are poorly understood. Icy cores that migrate over the water ice line can accrete a substantial amount of silicate material in giant impacts. This problem will be best addressed with *N*-body simulations that include pebbles and multiple protoplanets (e.g., Levison et al. 2015b). On the observational side, mass-radius relationships for observed super-Earths are degenerate in the relative amount of gaseous envelope and water content (Rogers & Seager 2010). Improved spectra of exoplanets, for example, with the *James Webb Space Telescope* that will be launched in 2018, will be needed to give better constraints on the relative contributions to the solid cores of super-Earths from icy material accreted exterior to the ice line and rocky material accreted interior to the ice line, to deduce the migration pathways of such planets.

DISCLOSURE STATEMENT

The authors are not aware of any affiliations, memberships, funding, or financial holdings that might be perceived as affecting the objectivity of this review.

ACKNOWLEDGMENTS

We would like to thank Bertram Bitsch and Alessandro Morbidelli for discussions that helped shaped this review. A.J. is grateful to Cornelis Dullemond, Hubert Klahr and Thomas Henning for discussions that helped develop the pebble accretion theory. A.J. thanks the Knut and Alice Wallenberg Foundation (grants 2012.0150, 2014.0017, 2014.0048), the Swedish Research Council (grant 2014-5775) and the European Research Council (ERC Starting Grant 278675-PEBBLE2PLANET) for their financial support. M.L. is grateful for support by the French ANR, project number ANR-1313-BS05-0003-01 (MOJO project—Modeling the Origin of JOvian planets).

LITERATURE CITED

Andrews SM, Wilner DJ, Hughes AM, Qi C, Dullemond CP. 2009. Protoplanetary disk structures in Ophiuchus. *Astrophys. J.* 700:1502–23

Bai XN, Stone JM. 2010. Dynamics of solids in the midplane of protoplanetary disks: implications for planetesimal formation. *Astrophys. J.* 722:1437–59

Baruteau C, Crida A, Paardekooper SJ, Masset F, Guilet J, et al. 2014. Planet-disk interactions and early evolution of planetary systems. In *Protostars and Planets VI*, ed. H Beuther, RS Klessen, CP Dullemond, T Hennig, pp. 667–89. Tucson: Univ. Ariz. Press

Benítez-Llambay P, Masset F, Koenigsberger G, Szulágyi J. 2015. Planet heating prevents inward migration of planetary cores. *Nature* 520:63–65

Benz W, Ida S, Alibert Y, Lin D, Mordasini C. 2014. Planet population synthesis. In *Protostars and Planets VI*, ed. H Beuther, RS Klessen, CP Dullemond, T Hennig, pp. 691–713. Tucson: Univ. Ariz. Press

Birnstiel T, Fang M, Johansen A. 2016. Dust evolution and the formation of planetesimals. *Space Sci. Rev.* 205:41–75

Birnstiel T, Klahr H, Ercolano B. 2012. A simple model for the evolution of the dust population in protoplanetary disks. *Astron. Astrophys.* 539:A148

Birnstiel T, Ormel CW, Dullemond CP. 2011. Dust size distributions in coagulation/fragmentation equilibrium: numerical solutions and analytical fits. *Astron. Astrophys.* 525:A11

Bitsch B, Johansen A. 2016. Influence of the water content in protoplanetary discs on planet migration and formation. *Astron. Astrophys.* 590:A101

Bitsch B, Johansen A, Lambrechts M, Morbidelli A. 2015a. The structure of protoplanetary discs around evolving young stars. *Astron. Astrophys.* 575:A28

Bitsch B, Lambrechts M, Johansen A. 2015b. The growth of planets by pebble accretion in evolving protoplanetary discs. *Astron. Astrophys.* 582:A112

Blum J, Wurm G. 2008. The growth mechanisms of macroscopic bodies in protoplanetary disks. *Annu. Rev. Astron. Astrophys.* 46:21–56

Boss AP. 2001. Gas giant protoplanet formation: disk instability models with thermodynamics and radiative transfer. *Astrophys. J.* 563:367–73

Bottke WF, Durda DD, Nesvorný D, Jedicke R, Morbidelli A, et al. 2005. The fossilized size distribution of the main asteroid belt. *Icarus* 175:111–40

Brauer F, Dullemond CP, Henning T. 2008. Coagulation, fragmentation and radial motion of solid particles in protoplanetary disks. *Astron. Astrophys.* 480:859–77

Brauer F, Dullemond CP, Johansen A, Henning T, Klahr H, Natta A. 2007. Survival of the mm-cm size grain population observed in protoplanetary disks. *Astron. Astrophys.* 469:1169–82

Buchhave LA, Latham DW, Johansen A, Bizzarro M, Torres G, et al. 2012. An abundance of small exoplanets around stars with a wide range of metallicities. *Nature* 486:375–77

Cameron AGW. 1978. Physics of the primitive solar accretion disk. *Moon Planets* 18:5–40

Carrera D, Johansen A, Davies MB. 2015. How to form planetesimals from mm-sized chondrules and chondrule aggregates. *Astron. Astrophys.* 579:A43

Chamberlin TC. 1916. The planetesimal hypothesis. *J. R. Astron. Soc. Can.* 10:473–97

Chambers JE. 2016. Pebble accretion and the diversity of planetary systems. *Astrophys. J.* 825:63

Chiang E, Laughlin G. 2013. The minimum-mass extrasolar nebula: in situ formation of close-in super-Earths. *MNRAS* 431:3444–55

Chiang E, Youdin AN. 2010. Forming planetesimals in solar and extrasolar nebulae. *Annu. Rev. Earth Planet. Sci.* 38:493–522

Coleman GAL, Nelson RP. 2016. On the formation of compact planetary systems via concurrent core accretion and migration. *MNRAS* 457:2480–500

Crida A, Morbidelli A. 2007. Cavity opening by a giant planet in a protoplanetary disc and effects on planetary migration. *MNRAS* 377:1324–36

D'Angelo G, Weidenschilling SJ, Lissauer JJ, Bodenheimer P. 2014. Growth of Jupiter: enhancement of core accretion by a voluminous low-mass envelope. *Icarus* 241:298–312

Dodson-Robinson SE, Veras D, Ford EB, Beichman CA. 2009. The formation mechanism of gas giants on wide orbits. *Astrophys. J.* 707:79–88

Drążkowska J, Alibert Y, Moore B. 2016. Close-in planetesimal formation by pile-up of drifting pebbles. *Astron. Astrophys.* 594:A105

Drążkowska J, Dullemond CP. 2014. Can dust coagulation trigger streaming instability? *Astron. Astrophys.* 572:A78

Drążkowska J, Windmark F, Dullemond CP. 2013. Planetesimal formation via sweep-up growth at the inner edge of dead zones. *Astron. Astrophys.* 556:A37

Fabrycky DC, Murray-Clay RA. 2010. Stability of the directly imaged multiplanet system HR 8799: resonance and masses. *Astrophys. J.* 710:1408–21

Fischer DA, Valenti J. 2005. The planet-metallicity correlation. *Astrophys. J.* 622:1102–17

Fressin F, Torres G, Charbonneau D, Bryson ST, Christiansen J, et al. 2013. The false positive rate of Kepler and the occurrence of planets. *Astrophys. J.* 766:81

Gorti U, Hollenbach D, Dullemond CP. 2015. The impact of dust evolution and photoevaporation on disk dispersal. *Astrophys. J.* 804:29

Gotberg Y, Davies MB, Mustill A, Johansen A, Church RP. 2016. Long-term stability of the HR 8799 planetary system without resonant lock. arXiv:1606.07819 [astro-ph.EP]

Greenberg R, Bottke WF, Carusi A, Valsecchi GB. 1991. Planetary accretion rates—analytical derivation. *Icarus* 94:98–111

Greenzweig Y, Lissauer JJ. 1990. Accretion rates of protoplanets. *Icarus* 87:40–77

Guillot T. 2005. The interiors of giant planets: models and outstanding questions. *Annu. Rev. Earth Planet. Sci.* 33:493–530

Guillot T, Ida S, Ormel CW. 2014. On the filtering and processing of dust by planetesimals. I. Derivation of collision probabilities for non-drifting planetesimals. *Astron. Astrophys.* 572:A72

Güttler C, Blum J, Zsom A, Ormel CW, Dullemond CP. 2010. The outcome of protoplanetary dust growth: pebbles, boulders, or planetesimals? I. Mapping the zoo of laboratory collision experiments. *Astron. Astrophys.* 513:A56

Hartmann L, Calvet N, Gullbring E, D'Alessio P. 1998. Accretion and the evolution of T Tauri disks. *Astrophys. J.* 495:385–400

Hayashi C. 1981. Structure of the solar nebula, growth and decay of magnetic fields and effects of magnetic and turbulent viscosities on the nebula. *Prog. Theor. Phys. Suppl.* 70:35–53

Hayashi C, Nakazawa K, Nakagawa Y. 1985. Formation of the solar system. In *Protostars and Planets II*, ed. DC Black, MS Matthews, pp. 1100–53. Tucson: Univ. Ariz. Press

Helled R, Bodenheimer P. 2014. The formation of Uranus and Neptune: challenges and implications for intermediate-mass exoplanets. *Astrophys. J.* 789:69

Helled R, Bodenheimer P, Podolak M, Boley A, Meru F, et al. 2014. Giant planet formation, evolution, and internal structure. In *Protostars and Planets VI*, ed. H. Beuther, RS Klessen, CP Dullemond, T Henning, pp. 643–66. Tucson: Univ. Ariz. Press

Ida S, Guillot T, Morbidelli A. 2016. The radial dependence of pebble accretion rates: a source of diversity in planetary systems. I. Analytical formulation. *Astron. Astrophys.* 591:A72

Ikoma M, Nakazawa K, Emori H. 2000. Formation of giant planets: dependences on core accretion rate and grain opacity. *Astrophys. J.* 537:1013–25

Johansen A, Blum J, Tanaka H, Ormel C, Bizzarro M, Rickman H. 2014. The multifaceted planetesimal formation process. In *Protostars and Planets VI*, ed. H. Beuther, RS Klessen, CP Dullemond, T Henning, pp. 547–70. Tucson: Univ. Ariz. Press

Johansen A, Lacerda P. 2010. Prograde rotation of protoplanets by accretion of pebbles in a gaseous environment. *MNRAS* 404:475–85

Johansen A, Mac Low MM, Lacerda P, Bizzarro M. 2015. Growth of asteroids, planetary embryos, and Kuiper belt objects by chondrule accretion. *Sci. Adv.* 1:1500109

Johansen A, Oishi JS, Mac Low MM, Klahr H, Henning T, Youdin A. 2007. Rapid planetesimal formation in turbulent circumstellar disks. *Nature* 448:1022–25

Johansen A, Youdin A. 2007. Protoplanetary disk turbulence driven by the streaming instability: nonlinear saturation and particle concentration. *Astrophys. J.* 662:627–41

Johansen A, Youdin A, Mac Low MM. 2009. Particle clumping and planetesimal formation depend strongly on metallicity. *Astrophys. J.* 704:L75–79

Kary DM, Lissauer JJ, Greenzweig Y. 1993. Nebular gas drag and planetary accretion. *Icarus* 106:288–307

Kretke KA, Levison HF. 2014. Challenges in forming the Solar System's giant planet cores via pebble accretion. *Astron. J.* 148:109

Krijt S, Ormel CW, Dominik C, Tielens AGGM. 2015. Erosion and the limits to planetesimal growth. *Astron. Astrophys.* 574:A83

Lambrechts M, Johansen A. 2012. Rapid growth of gas-giant cores by pebble accretion. *Astron. Astrophys.* 544:A32

Lambrechts M, Johansen A. 2014. Forming the cores of giant planets from the radial pebble flux in protoplanetary discs. *Astron. Astrophys.* 572:A107

Lambrechts M, Johansen A, Morbidelli A. 2014. Separating gas-giant and ice-giant planets by halting pebble accretion. *Astron. Astrophys.* 572:A35

Levison HF, Kretke KA, Duncan MJ. 2015a. Growing the gas-giant planets by the gradual accumulation of pebbles. *Nature* 524:322–24

Levison HF, Kretke KA, Walsh KJ, Bottke WF. 2015b. Growing the terrestrial planets from the gradual accumulation of sub-meter sized objects. *PNAS* 112:14180–85

Levison HF, Thommes E, Duncan MJ. 2010. Modeling the formation of giant planet cores. I. Evaluating key processes. *Astron. J.* 139:1297–314

Lin MK, Youdin AN. 2015. Cooling requirements for the vertical shear instability in protoplanetary disks. *Astrophys. J.* 811:17

Lissauer JJ. 1987. Timescales for planetary accretion and the structure of the protoplanetary disk. *Icarus* 69:249–65

Lissauer JJ, Fabrycky DC, Ford EB, Borucki WJ, Fressin F, et al. 2011. A closely packed system of low-mass, low-density planets transiting Kepler-11. *Nature* 470:53–58

Machida MN, Kokubo E, Inutsuka SI, Matsumoto T. 2010. Gas accretion onto a protoplanet and formation of a gas giant planet. *MNRAS* 405:1227–43

Marois C, Macintosh B, Barman T, Zuckerman B, Song I, et al. 2008. Direct imaging of multiple planets orbiting the star HR 8799. *Science* 322:1348

Marois C, Zuckerman B, Konopacky QM, Macintosh B, Barman T. 2010. Images of a fourth planet orbiting HR 8799. *Nature* 468:1080–83

Martin RG, Livio M. 2012. On the evolution of the snow line in protoplanetary discs. *MNRAS* 425:L6–9

Mayer L, Quinn T, Wadsley J, Stadel J. 2002. Formation of giant planets by fragmentation of protoplanetary disks. *Science* 298:1756–59

Mayor M, Marmier M, Lovis C, Udry S, Ségransan D, et al. 2011. The HARPS search for southern extra-solar planets XXXIV. Occurrence, mass distribution and orbital properties of super-Earths and Neptune-mass planets. arXiv:1109.2497 [astro-ph.EP]
Mizuno H. 1980. Formation of the giant planets. *Prog. Theor. Phys.* 64:544–57
Morbidelli A, Bitsch B, Crida A, Gounelle M, Guillot T, et al. 2016. Fossilized condensation lines in the Solar System protoplanetary disk. *Icarus* 267:368–76
Morbidelli A, Bottke WF, Nesvorný D, Levison HF. 2009. Asteroids were born big. *Icarus* 204:558–73
Morbidelli A, Lambrechts M, Jacobson S, Bitsch B. 2015. The great dichotomy of the Solar System: small terrestrial embryos and massive giant planet cores. *Icarus* 258:418–29
Morbidelli A, Nesvorny D. 2012. Dynamics of pebbles in the vicinity of a growing planetary embryo: hydrodynamical simulations. *Astron. Astrophys.* 546:A18
Musiolik G, Teiser J, Jankowski T, Wurm G. 2016. Collisions of CO_2 ice grains in planet formation. *Astrophys. J.* 818:16
Muto T, Inutsuka S. 2009. Orbital evolution of a particle interacting with a single planet in a protoplanetary disk. *Astrophys. J.* 695:1132–50
Nayakshin S. 2010. Formation of planets by tidal downsizing of giant planet embryos. *MNRAS* 408:L36–40
Nelson RP, Gressel O, Umurhan OM. 2013. Linear and non-linear evolution of the vertical shear instability in accretion discs. *MNRAS* 435:2610–32
Ogihara M, Morbidelli A, Guillot T. 2015. A reassessment of the in situ formation of close-in super-Earths. *Astron. Astrophys.* 578:A36
Okuzumi S, Tanaka H, Kobayashi H, Wada K. 2012. Rapid coagulation of porous dust aggregates outside the snow line: a pathway to successful icy planetesimal formation. *Astrophys. J.* 752:106
Ormel CW, Cuzzi JN. 2007. Closed-form expressions for particle relative velocities induced by turbulence. *Astron. Astrophys.* 466:413–20
Ormel CW, Klahr HH. 2010. The effect of gas drag on the growth of protoplanets. Analytical expressions for the accretion of small bodies in laminar disks. *Astron. Astrophys.* 520:A43
Ormel CW, Spaans M, Tielens AGGM. 2007. Dust coagulation in protoplanetary disks: porosity matters. *Astron. Astrophys.* 461:215–32
Paardekooper SJ, Baruteau C, Kley W. 2011. A torque formula for non-isothermal Type I planetary migration. II. Effects of diffusion. *MNRAS* 410:293–303
Piso AMA, Youdin AN. 2014. On the minimum core mass for giant planet formation at wide separations. *Astrophys. J.* 786:21
Pollack JB, Hubickyj O, Bodenheimer P, Lissauer JJ, Podolak M, Greenzweig Y. 1996. Formation of the giant planets by concurrent accretion of solids and gas. *Icarus* 124:62–85
Raettig N, Lyra W, Klahr H. 2013. A parameter study for baroclinic vortex amplification. *Astrophys. J.* 765:115
Rafikov RR. 2004. Fast accretion of small planetesimals by protoplanetary cores. *Astron. J.* 128:1348–63
Rogers LA, Seager S. 2010. Three possible origins for the gas layer on GJ 1214b. *Astrophys. J.* 716:1208–16
Ros K, Johansen A. 2013. Ice condensation as a planet formation mechanism. *Astron. Astrophys.* 552:A137
Safronov VS. 1969. *Evoliutsiia Doplanetnogo Oblaka.* Moscow: Nauka
Santos NC, Israelian G, Mayor M. 2004. Spectroscopic [Fe/H] for 98 extra-solar planet-host stars. Exploring the probability of planet formation. *Astron. Astrophys.* 415:1153–66
Schäfer U, Yang CC, Johansen A. 2017. Initial mass function of planetesimals formed by the streaming instability. *Astron. Astrophys.* 597:A69
Sheppard SS, Trujillo CA. 2010. The size distribution of the Neptune Trojans and the missing intermediate-sized planetesimals. *Astrophys. J.* 723:L233–37
Simon JB, Armitage PJ, Li R, Youdin AN. 2016. The mass and size distribution of planetesimals formed by the streaming instability. I. The role of self-gravity. *Astrophys. J.* 822:55
Stevenson DJ. 1982. Formation of the giant planets. *Planetary Space Sci.* 30:755–64
Tanaka H, Takeuchi T, Ward WR. 2002. Three-dimensional interaction between a planet and an isothermal gaseous disk. I. Corotation and Lindblad torques and planet migration. *Astrophys. J.* 565:1257–74
Testi L, Birnstiel T, Ricci L, Andrews S, Blum J, et al. 2014. Dust evolution in protoplanetary disks. In *Protostars and Planets VI*, ed. H. Beuther, RS Klessen, CP Dullemond, T Henning, pp. 339–61. Tucson: Univ. Ariz. Press

Testi L, Natta A, Shepherd DS, Wilner DJ. 2003. Large grains in the disk of CQ Tau. *Astron. Astrophys.* 403:323–28

Visser RG, Ormel CW. 2016. On the growth of pebble-accreting planetesimals. *Astron. Astrophys.* 586:A66

Wada K, Tanaka H, Suyama T, Kimura H, Yamamoto T. 2009. Collisional growth conditions for dust aggregates. *Astrophys. J.* 702:1490–501

Weidenschilling SJ, Davis DR. 1985. Orbital resonances in the solar nebula—implications for planetary accretion. *Icarus* 62:16–29

Wilner DJ, D'Alessio P, Calvet N, Claussen MJ, Hartmann L. 2005. Toward planetesimals in the disk around TW Hydrae: 3.5 centimeter dust emission. *Astrophys. J.* 626:L109–12

Wurm G, Paraskov G, Krauss O. 2005. Growth of planetesimals by impacts at ~25 m/s. *Icarus* 178:253–63

Wyatt MC. 2008. Evolution of debris disks. *Annu. Rev. Astron. Astrophys.* 46:339–83

Youdin AN, Chiang EI. 2004. Particle pileups and planetesimal formation. *Astrophys. J.* 601:1109–19

Youdin AN, Goodman J. 2005. Streaming instabilities in protoplanetary disks. *Astrophys. J.* 620:459–69

Youdin AN, Johansen A. 2007. Protoplanetary disk turbulence driven by the streaming instability: linear evolution and numerical methods. *Astrophys. J.* 662:613–26

Zsom A, Dullemond CP. 2008. A representative particle approach to coagulation and fragmentation of dust aggregates and fluid droplets. *Astron. Astrophys.* 489:931–41

Zsom A, Ormel CW, Güttler C, Blum J, Dullemond CP. 2010. The outcome of protoplanetary dust growth: pebbles, boulders, or planetesimals? II. Introducing the bouncing barrier. *Astron. Astrophys.* 513:A57

Annual Review
of Earth and
Planetary Sciences
Volume 45, 2017

Contents

Errata

An online log of corrections to *Annual Review of Earth and Planetary Sciences* articles may be found at http://www.annualreviews.org/errata/earth